Journal of Solid State Chemistry **148,** 260–277 (1999)
Article ID jssc.1999.8447, available online at http://www.idealibrary.com on IDEAL®

# Phase Transitions in the $Na_3M_2(PO_4)_2F_3$ Family ($M = Al^{3+}$, $V^{3+}$, $Cr^{3+}$, $Fe^{3+}$, $Ga^{3+}$): Synthesis, Thermal, Structural, and Magnetic Studies

J.-M. Le Meins,† M.-P. Crosnier-Lopez,* A. Hemon-Ribaud,* and G. Courbion*

*Laboratoire des Fluorures (UPRES-A 6010), Université du Maine, Faculté des Sciences, Avenue Olivier Messiaen, 72085 Le Mans Cedex 9, France; †Laboratoire de Matériaux Minéraux (UPRES-A 7016), Ecole Nationale Supérieure de Chimie de Mulhouse, 3, rue Alfred Werner, 68093 Mulhouse Cedex, France

Received January 26, 1999; in revised from July 12, 1999; accepted July 22, 1999

**The investigated compounds $Na_3M_2(PO_4)_2F_3$ ($M = Al^{3+}$, $V^{3+}$, $Cr^{3+}$, $Fe^{3+}$, $Ga^{3+}$) have been prepared by hydrothermal synthesis or by solid state synthesis and characterized by thermal analyses (TGA, DTA, DSC), powder and single crystal X-ray works, or neutron diffraction. Several other ways of characterization have also been used such as diffraction by TEM, IR, magnetism, and Mössbauer spectrometry. These compounds present two crystallographic transitions which involve three modifications: α, β, and α. The room temperature (β) phases can be split into two groups: the first ($\beta_1$), with $M = Al^{3+}$, $Cr^{3+}$, $Ga^{3+}$, crystallizes in the space group $P4_2/mbc$ ($a = 12.406(2)$ Å, $c = 10.411(2)$ Å, $Z = 8$ for $M = Al^{3+}$) whereas the second group ($\beta_3$) with $M = V^{3+}$, $Fe^{3+}$ crystallizes in the space group $P4_2/mnm$ ($a = 9.047(2)$ Å, $c = 10.705(2)$ Å, $Z = 4$ for $M = V^{3+}$). On the other hand all the high temperature (α) phases adopt the same space group $I4/mmm$ ($a = 6.206(1)$ Å, $c = 10.418(4)$ Å, $Z = 2$ for $M = Al^{3+}$). Mössbauer spectrometry and powder neutron diffraction (paramagnetic state) allowed us to evidence a low temperature (γ) phase on the Fe compound which is characterized by an orthorhombic symmetry ($a = 12.756(1)$ Å, $b = 12.803(1)$ Å, $c = 10.602(2)$ Å, $Z = 8$, space group *Pbam*). All these compounds adopt an identical three-dimensional $[M_2(PO_4)_2F_3]^{3-}_{\infty}$ network built up by sharing four corners between $PO_4$ tetrahedra and $M_2O_8F_3$ bioctahedra (one fluorine apex bridges two octahedra). $Na^+$ ions are statistically distributed inside the resulting channels. Susceptibility measurements reveal an antiferromagnetic behavior for each of the paramagnetic compounds ($M = V^{3+}$, $Cr^{3+}$, $Fe^{3+}$).** © 1999 Academic Press

***Key Words:*** **fluorides; fluorophosphates; phase transition; structure; magnetism.**

## INTRODUCTION

Many of known fluorophosphates are minerals. Among these, very few compounds involving monovalent cations ($Li^+$, $Na^+$, $K^+$) or divalent cations ($Ca^{2+}$, $Sr^{2+}$, $Ba^{2+}$) with trivalent ones ($Al^{3+}$ or 3*d* transition elements) have been discovered. The recent synthetic compounds are also few: $Na_5M(PO_4)_2F_2$ ($M^{3+}$ = Al, Cr, Ga) (1–3), $KM(PO_4)F$ ($M^{3+}$ = Al, Cr, Fe) (4–6), $Na_3Fe_2(PO_4)_2(OH)_2F$ (7), and $Na_3Fe_2(PO_4)_2F_3$ (8). During the investigation of the Na–Al–P–F–O system, to find optimum conditions of hydrothermal synthesis, we have isolated in a single crystal form the compound $Na_3Al_2(PO_4)_2F_3$ which presents a superstructure in relation to the known compounds with $M = Fe^{3+}$ (7, 8). So, we have studied the series with $M = V^{3+}$, $Cr^{3+}$, $Fe^{3+}$, and $Ga^{3+}$. We are presenting here the results of the phase transition study (mainly observed by thermal and diffraction experiments), then the structure determination of three polymorphs, and finally the magnetic behavior of the paramagnetic compounds (9).

## EXPERIMENTAL

### *Preparation*

The compounds were prepared as powders by solid state reactions by heating a mixture of (1) $3NaF–MPO_4$ or (2) $MF_3–MPO_4–Na_3PO_4$ in sealed gold or platinum tubes under argon atmosphere. After heating, the tubes are either air quenched or cooled down with a natural rate (about 200°/h). Crystals were also obtained by hydrothermal synthesis in the temperature range 630–710°C and high pressure (P ≈ 2000 bars) using a sealed platinum tube inserted in a steel autoclave for $M = Al^{3+}$ and $V^{3+}$. Flux growth technique can also be used for $M = Al^{3+}$ and $Fe^{3+}$. A typical flux of composition $3NaF–2MPO_4–0.9NaCl–0.6ZnCl_2$ was heated under argon atmosphere in a platinum crucible up to 700°C (12 h), then slowly cooled (6°C/h) down to 400°C and finally to room temperature at a rate of 20°C/h.

### *Characterisation*

Thermal analyses were performed by TGA and DTA on a T.A. apparatus between 30 and 1000°C under argon flow with a heating rate of 5°/min. DSC analyses were recorded



0022-4596/99 $30.00
Copyright © 1999 by Academic Press
All rights of reproduction in any form reserved.

on a Perkin Elmer DSC4 between $-200$ and $+100$°C at a scanning rate of 20°/min.

Powder X-ray diffraction patterns were performed, at room temperature, on a Siemens D500 diffractometer equipped with a diffracted beam graphite monochromator. Experiments at variable temperatures have been carried out on a Siemens D5000 diffractometer ($\theta/\theta$) equipped with a linear Elphyse detector and either a high temperature chamber (Anton Paar) or a low temperature chamber; the sample area was flowed by a stream of helium. In both cases, a Cu$K\alpha$ radiation was used. The powder neutron diffraction experiment was carried out at the LLB (Léon Brillouin Laboratory) on the G4.2 diffractometer ($\lambda = 2.597$ Å). The powder pattern was recorded between 2° to 160° $2\theta$ at a temperature of 80 K.

Electron microscopy experiments were performed on a JEOL 2010 electron microscope operating at 200 kV and equipped with a side entry $\pm 30°$ double tilt specimen holder. The thin specimens were prepared by grinding small crystals and then ultrasonically dispersing them in *n*-butanol. A few droplets of the suspension of $Na_3Al_2(PO_4)_2F_3$ were deposited on a carbon holey film supported by a Cu grid. A single tilt cryogenic specimen holder was also used to perform selected area electron diffraction (SAED) measurements.

Infrared spectra were collected on an ATI MATTSON Genesis spectrometer. Fluorine analyses were realized by the pyrohydrolysis method.

Magnetic susceptibility measurements were performed, in the temperature range 2.5–300 K, on a Faraday balance calibrated with a sample of cobalt mercurithiocyanate.

Single crystals were isolated under a polarizing microscope and the quality was then checked by Laue photographs. Data were collected on a Siemens–Stoe AED2 single crystal diffractometer at room temperature and with a Siemens–Nicolet single crystal diffractometer for lower temperatures ($-80$°C for example). The data were corrected for Lorentz-polarization and absorption effects (face indexing absorption correction was applied). The atomic scattering factors and anomalous dispersion correction were taken from International Tables for X-Ray Crystallography (10).

For structure determination programs SHELXS-86 (11), SHELXL-93 (12), JANA-96 (13), and FULLPROF (14) were used.

## RESULTS

### *Powder Synthesis*

Five compounds, $Na_3M_2(PO_4)_2F_3$ ($M = Al^{3+}$, $V^{3+}$, $Cr^{3+}$, $Fe^{3+}$, $Ga^{3+}$), were prepared. By solid state reactions, the best results were obtained with procedure (1) for $M = Al^{3+}$, $Cr^{3+}$, and $Fe^{3+}$.

For $M = Ga^{3+}$ and $V^{3+}$ the powder synthesis was achieved by a low temperature hydrothermal route (180°C, 30 bars). It can be pointed out that the $Na_3Ga_2(PO_4)_2F_3$ compound could not be synthesized without any impurities (such as $GaPO_4$, $GaF_3$ or other traces of unknown by-product). In the case of the $Na_3V_2(PO_4)_2F_3$ compound a specific route was followed. At first, a $V_2O_5$ powder, in phosphoric acid, is reduced by a $N_2H_4$–$H_2O$ solution to give a green solution ($V^{3+}$ ions). Then NaF is added in the following molar ratio: 4.3Na/2V and the solution is stirred for about 0.5 h and finally poured in a Teflon digestion bomb. Then, the whole mixture is introduced in a stainless-steel autoclave, heated at 180°C during 64 h, and slowly cooled down (10°/h) to room temperature.

Another way of synthesis for $M = Al^{3+}$, $Fe^{3+}$ was the recrystallization of fluorophosphate glasses. Indeed, vitreous domain in the system $NaPO_3$–$MF_3$ ($M$ = Al or Fe) was reported by Videau (15). We obtained the glass by heating the stoichiometric mixture ($3NaF$–$2MPO_4$) beyond the melting point in a sealed platinum tube followed by an air quenching. The Al glass, showing a larger temperature difference ($\Delta T$) between $T_c$ and $T_g$, is more stable than the Fe one. Taking into account the thermal behavior of these glasses, determined by DTA measurements, powder samples of $Na_3M_2(PO_4)_2F_3$ were obtained by heating the glass just above $T_c$ (for example: 12 h at 380°C for 1 g of Al sample).

### *Crystal Synthesis*

Single crystals were obtained for $M = Al^{3+}$, $V^{3+}$, and $Fe^{3+}$. The best result for $Al^{3+}$ and $V^{3+}$ was achieved by a hydrothermal route. Typical conditions for crystal growth are given in Table 1. For $Na_3V_2(PO_4)_2F_3$, the same procedure was used; the $H_3PO_4$ and solid mixture were replaced by the solution described in the previous paragraph.

Sometimes the crystals exhibit rather large dimensions (up to $1.5 \times 1.0 \times 0.8$ mm for $Na_3Al_2(PO_4)_2F_3$); they are colorless and green for $Al^{3+}$ and $V^{3+}$, respectively. For $M = Fe^{3+}$, the crystals obtained by a chloride flux method

**TABLE 1**
**Conditions for Hydrothermal Growth of $Na_3M_2(PO_4)_2F_3$**

| | $Al^{3+}$ | $V^{3+}$ |
|---|---|---|
| Volume of platinum tube | 3.27 ml | 2.88 ml |
| Filling level | 40% | 40% |
| Solvent | $H_3PO_4$ 7.4 M | $H_3PO_4/N_2H_4/H_2O$ (3/1/8.7) |
| Molar composition | $NaF/AlPO_4$ (6/1) | $NaF/V_2O_5$ (4/1) |
| Cold pressure | 100 MPa | 90 MPa |
| Heating rate | 200°/h | 200°/h |
| Maximum temperature | 707°C | 630°C |
| Maximum pressure | 218 MPa | 199 MPa |
| Dwell time at $T_{max.}$ | 24 h | 24 h |
| Cooling rate | 10°C/h | 10°C/h |

($SrF_2$–$FePO_4$–$ZnCl_2$–NaCl (1/1/2.0/1.6)) were also colorless.

### *Chemical Analysis and IR Spectra*

Several analyses were carried out in order to check the chemical formula $Na_3M_2(PO_4)_3F_2$ ($M$ = Al, V) of single crystals provided by hydrothermal synthesis. First, the sodium content was checked by atomic emission spectroscopy on few crushed crystals. For the Al compound an experimental weight percentage of 18.6(5)% (calculated: 18.6%) led to conclude that this phase is stoichiometric. Second, as hydrothermal route could lead to the substitution of F anions by hydroxyl OH groups, the possible OH content was checked by both fluorine analysis and IR spectra. A chemical analysis of fluorine by pyrohydrolysis method (16) led to an experimental weight percentage of 16.4(7)% for Al (calculated: 15.4%).

The IR spectra performed on crushed crystals for Al and V do not show any OH band around 3000–3500 $cm^{-1}$ (OH stretching) and are consistent with no substitution of F by OH. So the crystals prepared are fully fluorinated.

### *Phase Transition*

The X-ray diffraction patterns performed at room temperature on powder samples are very similar. On the force of it it seems that all the patterns can be indexed in a tetragonal cell with reflection conditions in agreement with space group $I4/mmm$ (No. 139). But the observation of small additional lines at different $d$ spacings is indicative of different unit cells related to phase transition.

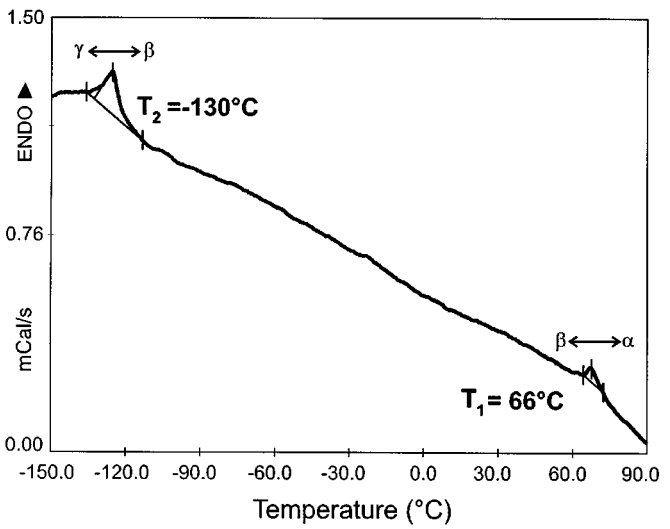


**FIG. 1.** DSC curve of $Na_3Cr_2(PO_4)_2F_3$ on heating up (heating rate: 5°C/min).

**TABLE 2**
**Melting Point and DSC Observed Temperatures of Allotropic Transitions in $Na_3M_2(PO_4)_2F_3$**

| $M^{3+}$ cation | Temperature (°C)[a] | Melting point (°C) |
|---|---|---|
| Al | $T_2 = 43(1)$ | 716(3) |
| Cr | $T_1 = -130(2)$, $T_2 = 66(2)$ | 1045(5) |
| Ga | $T_1 = -108(1)$ | 701(1) |
| Fe | $T_1 = -49(1)$ | 746(1) |

For the Cr compound, thermal analysis (DSC) clearly shows two reversible peaks (see Fig. 1), in relation with two phase transitions and three polymorphs called hereafter (on heating up) $\gamma$, $\beta$, and $\alpha$, at $T_1 = -130(2)$°C ($\gamma \leftrightarrow \beta$) and at $T_2 = 66(2)$°C ($\beta \leftrightarrow \alpha$). But only one significant peak is observed for the other cations (see Table 2). One of these transitions, $\beta \leftrightarrow \alpha$ ($T_2$), is easily observed by thermal X-ray diffraction (17) for three compounds: $V^{3+}$, $Cr^{3+}$, and $Al^{3+}$ (see Fig. 2 for $Na_3Al_2(PO_4)_2F_3$).

In the particular case of the $Fe^{3+}$ cation, the transition $\gamma \leftrightarrow \beta$ is clearly evidenced by DSC experiment ($T_1 = -49(2)$°C), but the one $\beta \leftrightarrow \alpha$ could only be estimated around 230(10)°C following a careful observation of the results of both DSC measurements and thermal X-ray diffraction experiments. Nevertheless, the $\gamma$ phase was evidenced by a powder neutron diffraction experiment performed in order to determine the magnetic structure. At −190°C, in the paramagnetic state, the powder pattern collected with a wavelength of 2.60 Å allowed us to point out the low temperature form ($\gamma$). This phase is characterized by the splitting of a few reflections present in $\beta$ (RT) form (Fig. 3). Such a splitting could not have been evidenced with a shorter wavelength such as Cu$K\alpha$. Mössbauer spectroscopy of $^{57}Fe$ (18) is the appropriate method that allows us to evidence the two transitions by following the evolution of the quadrupolar splitting parameter (QS) versus temperature (Fig. 4). The transition temperatures were found at −53 and 220°C, respectively, for $\gamma \leftrightarrow \beta$ and $\beta \leftrightarrow \alpha$.

The temperature and the experimental technique used to highlight the phase transition versus the nature of the cation are summarized in Table 3.

### *Cell Relations between Polymorphs*

Figure 5 shows the metric relations between the three different unit cells $\alpha$, $\beta$, and $\gamma$: $\alpha$ and $\beta$ are tetragonal whereas $\gamma$ is orthorhombic. At room temperature all the compounds are in the $\beta$ form (RT) (this explains the additional lines observed). Their cell parameters are reported in Table 4 (few impurities in the Ga compound do not allow us to describe it in the $\beta$ form). Both Fig. 5 and Table 4 point out the fact that this $\beta$ form is not the same whatever the cation is.

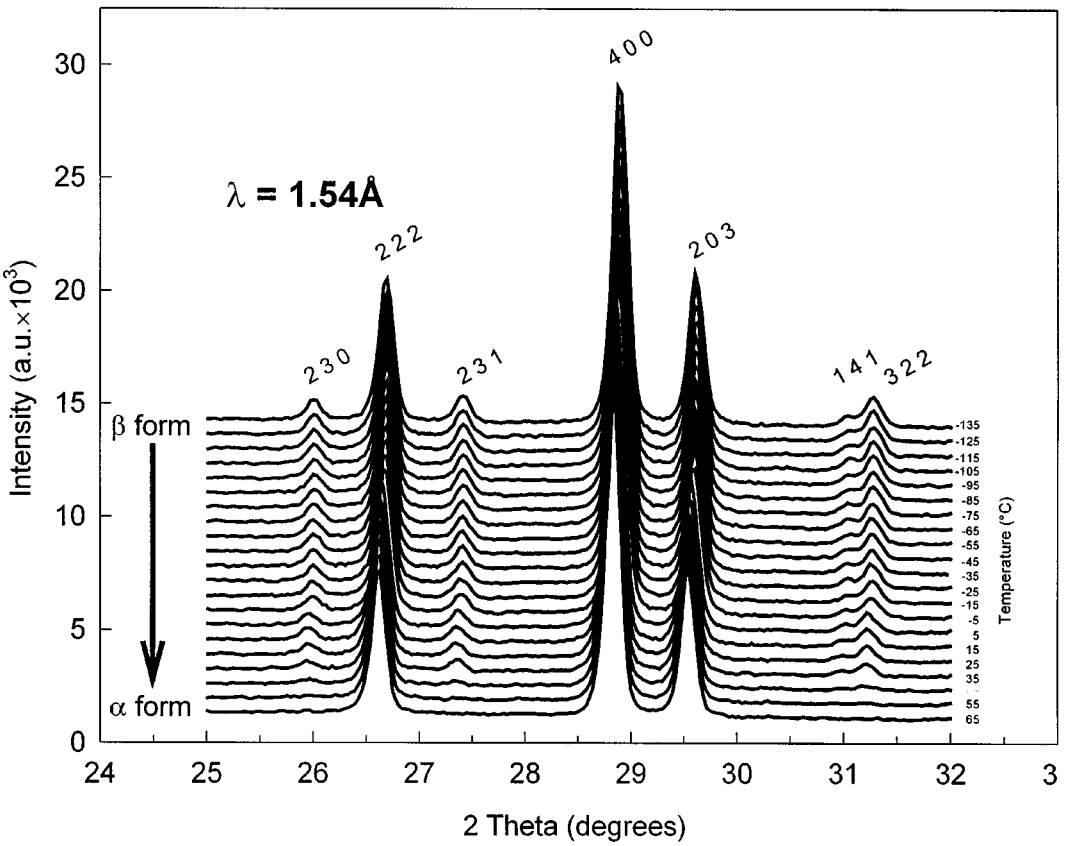


**FIG. 2.** Thermal X-ray diffraction experiment (Cu$K\alpha$) carried out on $Na_3Al_2(PO_4)_2F_3$. The additional small reflections characterize the $\beta$ form (Miller indices are given in the $P4_2/mbc$ space group).

Indeed, two kinds of superstructure are evidenced, one for the smaller cations $Al^{3+}$ and $Cr^{3+}$ ($V_{\beta 1} \approx 4V_\alpha$), the other for the larger ones $Fe^{3+}$ and $V^{3+}$ ($V_{\beta 2} \approx 2V_\alpha$). No conclusion is available with the Ga compound because of small impurities which make it impossible to achieve any classification. For the $\gamma$ cell, the simple relation $V_{\beta 1} \approx V\gamma$) is observed.

A particular study of the Al compound (single crystals) was carried out by means of electron diffraction. The reciprocal lattice construction (program TILT-MET (19)) indicates, at room temperature, a body-centered tetragonal Bravais lattice with $a = 6.2(3)$ Å, $c = 10.4(4)$ Å. The values of these parameters are coherent with those of the $\alpha$ form. This first approach leads us to evidence the $\alpha$ (HT) form at room temperature. Yet, it is quite interesting to notice that one of the diffraction patterns which allowed us to build the reciprocal lattice presents diffuse streaks suggesting a superstructure. With a single tilt cryogenic specimen holder several SAED measurements have been collected and the reciprocal plane ($a^*$, $b^*$), oriented almost perfectly, has even been observed. Some diffraction spots appear very clearly, indicating the presence of a superstructure with the $a$ parameter doubled ($a' = 12.4(3)$ Å). The crystal system remains unchanged, but the Bravais lattice becomes P. Such results are consistent with the existence of two modifications $\alpha$ (HT) and $\beta_1$ (RT). For this Al compound, the transition temperature $\beta_1 \leftrightarrow \alpha$ is close to room temperature ($T_2 = 43°C$). In order to confirm the proposed supercell ($\beta_1$), X-ray powder patterns were recorded from room temperature down to $-100°C$. The intensity of the additional reflections increases on cooling down and a progressive saturation appears around $-80°C$ (Fig. 6). Consequently, we decided to collect data on the single crystal at $T = -80°C$ for the structure determination of the $\beta_1$ form of $Na_3Al_2(PO_4)_2F_3$.

## STRUCTURE DETERMINATION

Crystals corresponding to $M = Al^{3+}$ and $M = V^{3+}$ were studied. Fortunately, two kinds of crystals were observed for the Al species: some were frozen in the $\alpha$-form and the others exhibited the superstructure reflections of the $\beta$-form. In fact, four data collections were made, three for $M = Al^{3+}$

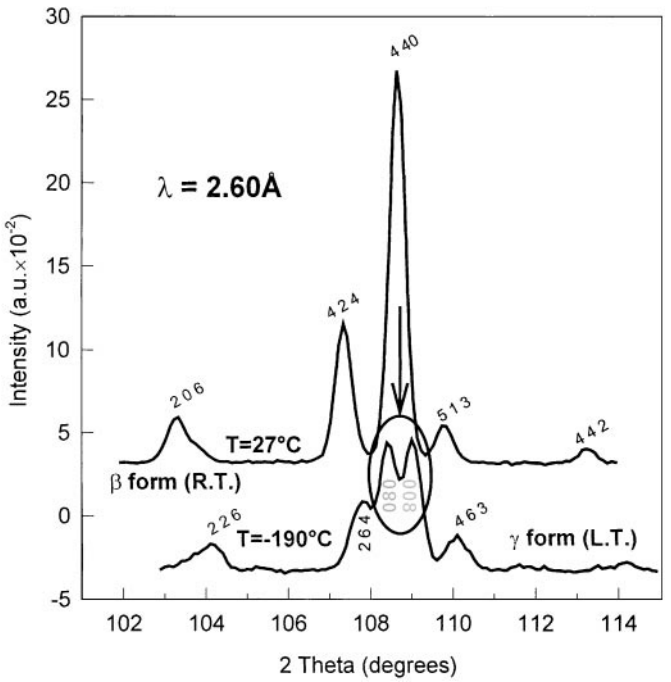


**FIG. 3.** Neutron powder patterns of $Na_3Fe_2(PO_4)_2F_3$ at room temperature and $-190°C$ (paramagnetic state). The superstructure ($\gamma$ form) is mainly evidenced by the splitting of the 440 line space group ($P4_2/mnm$ at 27°C and $Pbam$ at $-190°C$).

($\alpha$-form, $\beta$-form at $T = 20°C$, $\beta$-form at $T = -80°C$) and one for $M = V^{3+}$ in the $\beta$-form. The $\gamma$-form was studied for $M = Fe^{3+}$ by means of a neutron diffraction experiment on powder sample. The conditions of data collection are summarized in Table 5 for $M = Al^{3+}$ and $V^{3+}$, and in Table 12 for $M = Fe^{3+}$. A list of observed and calculated structure factors can be obtained from the authors upon request.

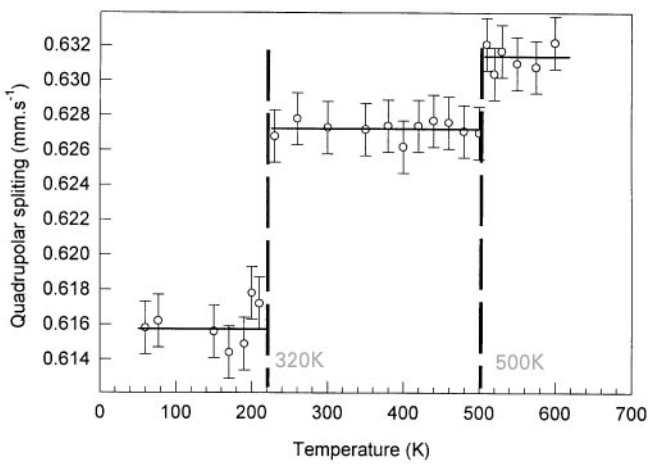


**FIG. 4.** Temperature dependence of the quadrupolar splitting at $^{57}Fe$ in $Na_3Fe_2(PO_4)_2F_3$.

**TABLE 3**
**Summary of the Different Transitions Evidenced in this Work versus the Cation, with the Associated Method of Investigation (Temperatures Given in °C.)**

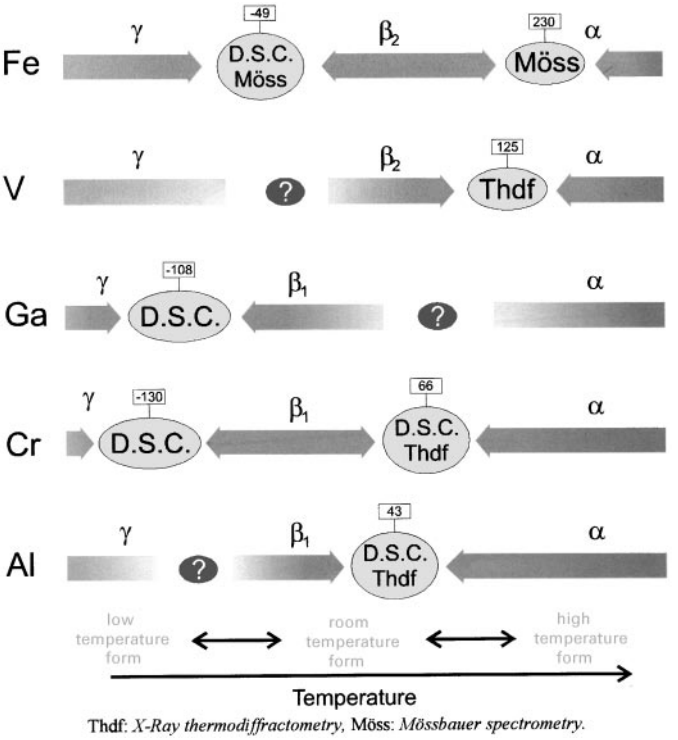


## $\alpha$-$Na_3Al_2(PO_4)_2F_3$ (*High Temperature Form*)

At the beginning of this work, no result was reported about an isotypic compound in space group $I4/mmm$. The structure was solved by Patterson techniques using the program SHELXS-86. P and Al atoms were located first. Then the refinement was led by the JANA-96 program. The anions were placed on a criteria of distances and the resulting difference Fourier map clearly shows two important residuals localized on two special positions of the group: 8*h* and 8*j*. These peaks were attributed to Na atoms. The

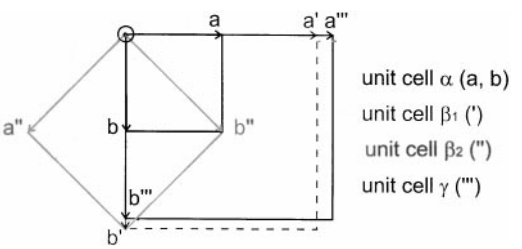


**FIG. 5.** Metric relations between the different unit cells of each variety $\alpha$, $\beta_1$, $\beta_2$, and $\gamma$.

**TABLE 4**
**Cell Parameters for Different Phases $Na_3M_2(PO_4)_2F_3$ ($M = Al^{3+}$, $V^{3+}$, $Cr^{3+}$, $Fe^{3+}$, $Ga^{3+}$) at Room Temperature (from X-Ray Powder Patterns)**

| $M^{3+}$ cation | $a$ (Å) | $c$ (Å) | $V$ (Å$^3$) | Parameter relation | Volume relation |
|---|---|---|---|---|---|
| Al | 12.404(2) | 10.410(2) | 1602(1) | $a' = 2a$, $c' = c$ | $V(\beta_1) = 4V(\alpha)$ |
| Ga[(1)] | 6.291(1) | 10.646(1) | 421(1) | — | — |
| Cr | 12.666(2) | 10.608(2) | 1702(1) | $a' = 2a$, $c' = c$ | $V(\beta_1) = 4V(\alpha)$ |
| V | 9.041(2) | 10.737(2) | 878(1) | $a'' = a\sqrt{2}$, $c'' = c$ | $V(\beta_2) = 2V(\alpha)$ |
| Fe | 9.037(2) | 10.668(2) | 871(1) | $a'' = a\sqrt{2}$, $c'' = c$ | $V(\beta_2) = 2V(\alpha)$ |

*Note*. Metric relations with $\alpha$ cell.
[a] Given in the $\alpha$ form at room temperature.

resulting formula "$Na_8Al_2(PO_4)_2F_3$" and the too large values for the equivalent atomic displacement parameter (ADP) of the two Na atoms ($B_{eq} = 6.5$ Å$^2$ for Na(1) and 20.5 Å$^2$ for Na(2)) led us to refine the site occupation factors for sites 8*h* and 8*j* which respectively converge around $\frac{1}{2}$ and $\frac{1}{4}$ (resulting chemical formula $Na_3Al_2(PO_4)_2F_3$). So, the solution suggested in this study is established from a harmonic model with Na atoms statistically distributed on two sites (8*j* and 8*h*). Consequently, the equivalent ADPs take more convenient values: 3.0(1) and 9(1) Å$^2$ for Na(1) and Na(2), respectively. Successive refinements made the reliability factors drop to $R_1 = 2.70\%$, $\omega R_2 = 8.00\%$, and led to 5.7(2) Na instead of the 6 expected. The result is rather similar to the structure proposed recently for $Na_3Fe_2(PO_4)_2F_3$ and $Na_3Al_2(PO_4)_2F_3$ by Yakubovitch *et al.* (8, 20), except that these authors proposed three different atomic positions for the Na species. One consequence of such a model results in the decrease of the equivalent ADPs associated to these cations. In our refinement, we can notice that the maximum of electronic density remaining ($1.57e^-$/Å$^3$) is actually on the position selected by Yakubovitch *et al.* for the third $Na^+$ cation. Nevertheless, this involves a very short distance between Na(1) and Na(3): 0.394 Å. Such a distance is close to the resolution allowed by the diffractometer we used and dissuaded us from going further in this model. A nonharmonic development of the Debye–Waller factor of Na(1) allows the improvement of the modelization of the electronic density around this atom and shows that only two sites for the Na species are efficient (21).

The atomic parameters are given in Table 6 for two Na sites (with a classical harmonic development of the associated Debye–Waller factor to each site) and the main distances and angles are listed in Table 7.

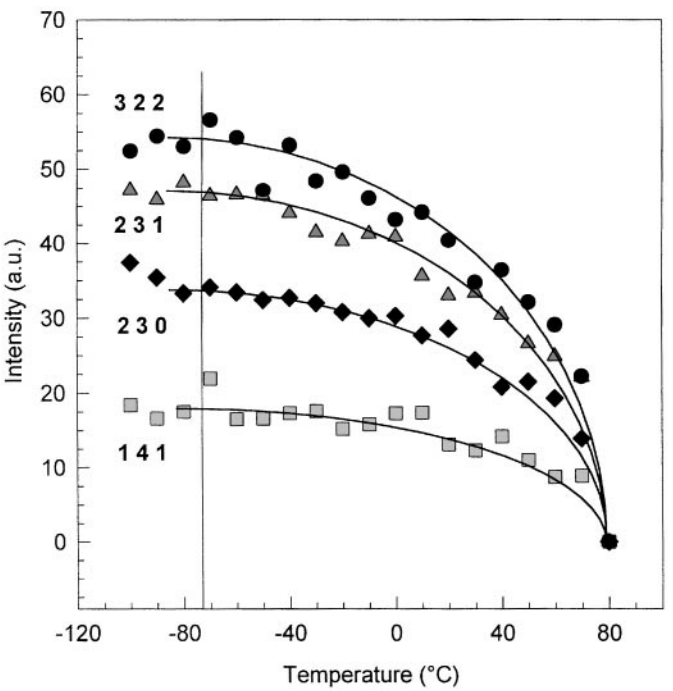


**FIG. 6.** Intensity of the main reflections of superstructure for $Na_3Al_2(PO_4)_2F_3$ versus temperature, (space group $P4_2/mbc$).

## $\beta_1$-$Na_3Al_2(PO_4)_2F_3$ (*Room Temperature Form*)

Cell characterization at room temperature of another $Na_3Al_2(PO_4)_2F_3$ crystal by X-ray diffraction with a fast scan leads the first time to the tetragonal cell in the space group $I4/mmm$ (HT form) while a study with a slow scan of weak reflections leads to the tetragonal cell—$a' = 12.406(2)$ Å, $c' = 10.411(2)$ Å—with systematic extinction conditions consistent with centrosymmetric space group $P4_2/mbc$. A careful examination of observed intensities revealed the superstructure existence, because 43% of reflections with even $h$ and $k$ were kept ($I > 3\sigma(I)$) whereas only 9% with odd $h$ and/or $k$ were kept. Moreover, the most intense with odd $h$ and $k$ has an intensity which represents only 1% of the greater reflection. These results are consistent with the electron diffraction experiments by TEM which clearly revealed the existence of tetragonal cell with $a' = 2a$.

Data collection in the $a'$, $c'$ cell has been realized on the same crystal at room temperature and at $-80$°C. The $I4/mmm$ structural model with two sodium atoms sites (8*j*, 8*h*) was extended to the supercell using space group $P4_2/mbc$ with a correct choice of origin. The 8*j* and 8*h* sites of $I4/mmm$ give rise to four 8*h* sites in the supercell.

The atomic coordinates and thermal parameters are listed in Table 8 for $T = 20$ and $-80$°C. Some characteristic distances and angles are also given in Table 9.

The main difference between the two structural results ($T = 20$ and $-80$°C) comes from the distribution of

**TABLE 5**
**Crystallographic Data for $Na_3M_2(PO_4)_2F_3$**

| | | | | |
|---|---|---|---|---|
| | | Crystal data | | |
| Formula | $\alpha$-$Na_3Al_2(PO_4)_2F_3$ | $\beta_1$-$Na_3Al_2(PO_4)_2F_3$ | $\beta_1$-$Na_3Al_2(PO_4)_2F_3$ | $\beta_2$-$Na_3V_2(PO_4)_2F_3$ |
| Crystal system | tetragonal | tetragonal | tetragonal | tetragonal |
| Cell dimensions | $a = 6.206(1)$ Å | $a' = 12.406(2)$ Å | $a' = 12.382(2)$ Å | $a = 9.047(2)$ Å |
| | $c = 10.418(4)$ Å | $c' = 10.411(2)$ Å | $c' = 10.387(2)$ Å | $c = 10.705(2)$ Å |
| Volume | $V = 401.2(2)$ Å$^3$ | $V = 1602.4(5)$ Å$^3$ | $V = 1592.5(8)$ Å$^3$ | $V = 876.2(3)$ Å$^3$ |
| $Z$ | 2 | 8 | 8 | 4 |
| Space group | $I4/mmm$ (No. 139) | $P4_2/mbc$ (No.135) | $P4_2/mbc$ (No.135) | $P4_2/mnm$ (No.136) |
| Calculated density | 3.06 | 3.06 | 3.09 | 3.17 |
| | | Intensity measurements | | |
| Temperature (°C) | 20 | 20 | − 80 | 20 |
| $\lambda$ (Mo$K\alpha$) | 0.71073 Å | 0.71073 Å | 0.71073 Å | 0.71073 Å |
| Scan mode | $\omega/2\theta$ | $\omega/2\theta$ | | |
| Crystal size (mm$^3$) | 0.005 | 0.05 | 0.05 | 0.001 |
| Linear absorption coeff. (cm$^{-1}$) | 10.4 | 10.4 | 10.4 | 28.4 |
| Recording range $2\theta$ (°) | 4–90 | 4–70 | 4–70 | 4–90 |
| $hkl$ range | $h^{-12}_{+12}$, $k^{-8}_{+8}$, $l^{0}_{20}$ | $h^{-20}_{+20}$, $k^{-9}_{14}$, $l^{0}_{16}$ | $h^{0}_{18}$, $k^{0}_{18}$, $l^{-16}_{+16}$ | $h^{-6}_{+14}$, $k^{-14}_{+17}$, $l^{-17}_{+21}$ |
| No. of measured reflections | 1122 | 1457 | 3570 | 2675 |
| | | Data reduction | | |
| No. of independent reflections | 523 | 1296 | 1348 | 1411 |
| $R_{int}$ | 0.019 | 0.006 | 0.095 | 0.025 |
| Absorption correction | No | Yes | Yes | Yes |
| Transmission coefficient | 0.80/0.92 | 0.59/0.87 | 0.59/0.87 | 0.88/0.96 |
| Reflections with $I > 2\sigma(I)$ | 452 | 532 | 1014 | 585 |
| | | Refinement | | |
| Parameters refined | 28 | 128 | 128 | 57 |
| Agreement factors | $R_1 = 0.027$, $\omega R_2 = 0.080$ | $R_1 = 0.032$, $\omega R_2 = 0.15$ | $R_1 = 0.067$, $\omega R_2 = 0.24$ | $R_1 = 0.047$, $\omega R_2 = 0.084$ |
| Weighting scheme | unstab coefficient: 1.5[a] | $\omega = 1/[\sigma^2(F_o^2) + (0.081P)^2]$[b] | $\omega = 1/[\sigma^2(F_o^2) + (0.177P)^2 + 8.45P]$[b] | unstab. coefficient: 0.8[a] |
| Secondary extinction | type I extinction, $g_{iso} = 0.21(3)$[a] | $x = 0.011(1)$[b] | $x = 0.056(4)$[b] | type I extinction, $g_{iso} = 0.12(1)$[a] |
| Difference Fourier residues | [ − 1.57; + 1.57] e$^-$/Å$^3$ | [ − 0.95; + 0.73] e$^-$/Å$^3$ | [ − 2.51; + 2.12] e$^-$/Å$^3$ | [ − 4.39; + 3.80] e$^-$/Å$^3$ |

*Note*. As defined in [a] JANA-96 and [b] SHELXL-93.

sodium atom sites. At room temperature, the eight sites are slightly shifted in relation to the symmetrical model in the $I4/mmm$ space group ($\alpha$-form), whereas at lower temperature rather important shifts (ranging from 0.3 to 0.5 Å) and nonsymmetrical distribution are noticed. Figure 7 shows the distributions of sodium atoms over their sites in both forms ($\alpha$ and $\beta_1$) and at both temperatures for $\beta_1$.

### $\beta_2$-$Na_3V_2(PO_4)_2F_3$ (*Room Temperature Form*)

Cell characterization at room temperature of a $Na_3V_2(PO_4)_2F_3$ crystal by X-ray diffraction leads to the tetragonal cell—$a'' = 9.047(2)$ Å, $c'' = 10.705(2)$ Å—and observed systematic extinctions are consistent with centrosymmetric space group $P4_2/mnm$. The data collection conditions are summarized in Table 5. This tetragonal cell has been already encountered in the $Na_3Fe_2(PO_4)_2(OH)_2F$ compound by Yakubovich *et al.* (7). The crystal structure was refined from the proposed structural model with two sites for the Na atoms. Strong ADP values and unbalanced chemical formula $Na_4V_2(PO_4)_2F_3$ lead us to refine the site

**TABLE 6**
**Atomic Parameters and Equivalent Isotropic Displacement Parameters (Å$^2$) for $\alpha$-$Na_3Al_2(PO_4)_2F_3$ at Room Temperature (space group $I4/mmm$)**

| Atom | Site | sof | $x$ | $y$ | $z$ | $B_{eq}$ |
|---|---|---|---|---|---|---|
| Na(1) | 8$h$ | 0.124(3) | 0.2823(3) | 0.2823(3) | 0 | 3.0(1) |
| Na(2) | 8$j$ | 0.052(3) | $\frac{1}{2}$ | 0.226(1) | 0 | 9(1) |
| Al | 4$e$ | 0.125 | 0 | 0 | 0.17930(6) | 0.442(8) |
| P | 4$d$ | 0.125 | 0 | $\frac{1}{2}$ | $\frac{1}{4}$ | 0.366(6) |
| O | 16$n$ | 0.5 | 0 | 0.3026(1) | 0.16185(7) | 0.789(1) |
| F(1) | 2$a$ | 0.0625 | 0 | 0 | 0 | 0.60(2) |
| F(2) | 4$e$ | 0.125 | 0 | 0 | 0.3543(1) | 0.97(1) |

**TABLE 7**
**Main Interatomic Distances (Å) and Angles (°) for α-$Na_3Al_2(PO_4)_2F_3$**

Al Octahedron

| Al | O | O | O | O | F(1) | $F(2)^{terminal}$ |
|---|---|---|---|---|---|---|
| O | **1.887(1)** | 3.757(2) | 2.656(2) | 2.656(2) | 2.524(2) | 2.750(2) |
| O | 168.98(4) | **1.887(1)** | 2.656(2) | 2.656(2) | 2.524(2) | 2.750(2) |
| O | 89.47(4) | 84.49(4) | **1.887(1)** | 2.656(2) | 2.524(2) | 2.750(2) |
| O | 89.47(4) | 89.47(4) | 89.47(2) | **1.887(1)** | 2.524(2) | 2.750(2) |
| F(1) | 84.49(2) | 84.49(2) | 84.49(2) | 84.49(2) | **1.867(1)** | 3.693(2) |
| $F(2)^{terminal}$ | 95.51(2) | 95.51(2) | 95.51(2) | 95.51(2) | 180 | **1.823(1)** |

⟨Al—O, F⟩ 1.87 Å, $d_{Shannon}$ 1.86 Å

P Tetrahedron

| P | O | O | O | O |
|---|---|---|---|---|
| O | **1.531(1)** | 2.525(2) | 2.449(1) | 2.525(2) |
| O | 111.1(2) | **1.531(1)** | 2.525(2) | 2.449(1) |
| O | 106.2(2) | 111.1(2) | **1.531(1)** | 2.525(2) |
| O | 111.1(2) | 106.2(2) | 111.1(2) | **1.531(1)** |

⟨P—O⟩1.53 Å, $d_{Shannon}$ 1.52 Å

| Na(1) Polyhedron CN 7 | | Na(2) Polyhedron CN 6 | |
|---|---|---|---|
| Na(1)–O | 4 × 2.432(1) | | |
| Na(1)–F(1) | 1 × 2.472(2) | Na(2)–F(2) | 2 × 2.280(5) |
| Na(1)–F(2) | 2 × 2.444(2) | Na(2)–O | 4 × 2.512(3) |
| **⟨Na–O, F⟩** | **2.44** | **⟨Na–O, F⟩** | **2.43** |
| | | $d_{Shannon}$ 2.45 Å | |

Shorter distances characterizing the disorder of $Na^+$ cations

| | |
|---|---|
| Na(1)–Na(2) | 1.40(1) Å |
| Na(2)–Na(2) | 2.41(1) Å |

occupation factor (sof) of one of the Na atoms (Na(2)). After several cycles of calculation, the sof converges toward 0.249(4) and finally this value is fixed to 0.25 following Yakubovich's result ($Na_3V_2(PO_4)_2F_3$). At the end of the refinement, the reliability factors dropped to $R_1 = 4.76\%$ for 585 $F_o > 4\sigma(F_o)$ and $\omega R_2 = 8.43\%$ for 1411 independent reflections. The final atomic coordinates and equivalent ADPs are listed in Table 10 and some characteristic distances and angles are given in Table 11.

### γ-$Na_3Fe_2(PO_4)_2F_3$ (*Low Temperature Form*)

The room temperature structure ($\beta_2$ form) has been determined by both single crystal and powder diffraction. The results are similar to those obtained for the $V^{3+}$ compound and confirm the structure established by Yakubovitch *et al.* (7).

At low temperature, the study has been carried out on powder sample by neutron diffraction. The data have been collected at −190°C in the paramagnetic state. Few traces of impurities (α-$Fe_2O_3$ and $Na_3Fe_2(PO_4)_3$) were detected on the diffractogram (Fig. 8) (22). However, their reflections (very weak) do not match with those of the studied compound and they do not disturb the structure determination. In a first approach, the structure was studied in space group $P4_2/mnm$, i.e., in the $\beta_2$ form. Such a proposition was systematically rejected during the refinement cycles with the FULLPROF program. As said previously, the diffraction pattern reveals that some reflections are not indexed in the tetragonal unit cell of the $\beta_2$ form. Two kinds of new reflections are noticed: those missed at 300 K or those issued from a splitting of reflections already present at room temperature (Fig. 3). A new unit cell with an orthorhombic symmetry is proposed to take such reflections into account. The extinction conditions are consistent with *Pbam* space group and the structure determination is carried out on the

**TABLE 8**
**Atomic Parameters and Equivalent Isotropic Displacement Parameters (Å²) for $\beta_1$-$Na_3Al_2(PO_4)_2F_3$ at 20 and −80°C**

| Atom | Site | sof (−80°C) | sof (20°C) | x (−80°C) | x (20°C) | y (−80°C) | y (20°C) | z (−80°C) | z (20°C) | $B_{eq}$ (−80°C) | $B_{eq}$ (20°C) |
|---|---|---|---|---|---|---|---|---|---|---|---|
| Na(1) | 8*h* | 0.315(4) | 0.270(4) | 0.3733(2) | 0.3674(4) | 0.5961(3) | 0.6030(2) | 0 | 0 | 0.95(5) | 2.5(1) |
| Na(2) | 8*h* | 0.333(5) | 0.249(5) | 0.1302(2) | 0.1381(3) | 0.5984(3) | 0.6063(4) | 0 | 0 | 0.84(5) | 2.1(1) |
| Na(3) | 8*h* | 0.093(5) | 0.208(5) | 0.1348(8) | 0.1487(4) | 0.3288(25) | 0.3843(6) | 0 | 0 | 4.6(6) | 3.4(2) |
| Na(4) | 8*h* | 0.217(4) | 0.216(4) | 0.3406(3) | 0.3564(5) | 0.3761(3) | 0.3896(4) | 0 | 0 | 0.85(6) | 3.6(2) |
| Na(5) | 8*h* | 0.222(4) | 0.114(4) | 0.3925(4) | 0.3936(5) | 0.5055(3) | 0.5024(6) | 0 | 0 | 1.8(1) | 3.7(4) |
| Na(6) | 8*h* | 0.051(6) | 0.159(8) | 0.1095(16) | 0.1122(17) | 0.5075(3) | 0.5139(5) | 0 | 0 | 3.0(7) | 13(1) |
| Na(7) | 8*h* | 0.237(4) | 0.184(6) | 0.2513(4) | 0.2547(3) | 0.3579(2) | 0.3638(12) | 0 | 0 | 1.45(7) | 7.7(6) |
| Na(8) | 8*h* | 0.180(5) | 0.160(6) | 0.3417(4) | 0.2611(6) | 0.6264(4) | 0.6318(32) | 0 | 0 | 0.65(8) | 22(2) |
| Al | 16*i* | 1 | 1 | 0.00010(4) | −0.00003(2) | 0.2489(6) | 0.24989(6) | 0.1793(1) | 0.17922(5) | 0.45(2) | 0.45(2) |
| P(1) | 4*b* | 0.25 | 0.25 | 0 | 0 | 0 | 0 | 0.25 | 0.25 | 0.44(4) | 0.40(2) |
| P(2) | 4*d* | 0.25 | 0.25 | 0 | 0 | 0.5 | 0.5 | 0.25 | 0.25 | 0.44(4) | 0.42(2) |
| P(3) | 8*g* | 0.5 | 0.5 | 0.24807(4) | 0.24936(2) | 0.74807(4) | 0.74936(2) | 0.25 | 0.25 | 0.39(2) | 0.38(2) |
| F(1) | 8*h* | 0.5 | 0.5 | 0.0023(1) | 0.0082(6) | 0.2548(7) | 0.2503(2) | 0 | 0 | 0.46(4) | 0.51(2) |
| F(2) | 16*i* | 1 | 1 | −0.0033(1) | −0.00115(4) | 0.2451(5) | 0.2502(1) | 0.3545(2) | 0.3545(1) | 0.71(3) | 0.97(2) |
| O(1) | 16*i* | 1 | 1 | 0.1022(3) | 0.0991(1) | 0.0023(1) | 0.00117(5) | 0.3405(4) | 0.3372(2) | 0.63(6) | 0.80(3) |
| O(2) | 16*i* | 1 | 1 | 0.5956(3) | 0.5988(1) | 0.0008(1) | 0.00036(5) | 0.3369(5) | 0.3380(2) | 0.66(6) | 0.88(3) |
| O(3) | 16*i* | 1 | 1 | 0.2500(3) | 0.2508(1) | 0.3488(1) | 0.3486(1) | 0.3358(2) | 0.3372(2) | 0.70(2) | 0.76(3) |
| O(4) | 16*i* | 1 | 1 | 0.7564(2) | 0.7516(1) | 0.3490(1) | 0.3486(1) | 0.3415(2) | 0.3392(2) | 0.47(2) | 0.72(3) |

**TABLE 9**
**Main Interatomic Distances (Å) and Angles (°) for $\beta_1$-$Na_3Al_2(PO_4)_2F_3$ at 20°C and −80°C (gray)**

**Al Octahedron**

| Al | $F(2)^{terminal}$ | F(1) | O(1) | O(2) | O(3) | O(4) |
|---|---|---|---|---|---|---|
| $F(2)^{terminal}$ | **1.825(2)** | 3.691(2) | 2.743(2) | 2.743(2) | 2.750(1) | 2.746(1) |
| | **1.821(3)** | 3.685(3) | 2.691(5) | 2.800(3) | 2.751(4) | 2.741(2) |
| F(1) | 179.7(1) | **1.866(1)** | 2.525(3) | 2.519(1) | 2.522(2) | 2.524(3) |
| | 179.1(5) | **1.864(1)** | 2.514(3) | 2.511(6) | 2.512(1) | 2.512(5) |
| O(1) | 95.5(1) | 84.8(1) | **1.879(1)** | 3.747(3) | 2.654(3) | 2.657(3) |
| | 95.0(3) | 85.8(4) | **1.829(9)** | 3.743(5) | 2.610(4) | 2.653(3) |
| O(2) | 95.4(1) | 84.4(1) | 169.1(1) | **1.885(2)** | 2.658(1) | 2.643(1) |
| | 96.5(4) | 82.8(1) | 168.5(1) | **1.933(9)** | 2.668(8) | 2.626(1) |
| O(3) | 95.6(1) | 84.5(1) | 89.6(1) | 89.6(1) | **1.886(1)** | 3.756(1) |
| | 96.1(1) | 84.3(1) | 90.8(3) | 88.9(1) | **1.877(1)** | 3.743(3) |
| O(4) | 95.4(1) | 84.5(1) | 89.7(1) | 89.0(1) | 169.0(1) | **1.888(1)** |
| | 95.4(1) | 84.1(1) | 91.1(2) | 86.9(2) | 168.5(1) | **1.886(2)** |

**<Al-O, F> = 1.87Å,** 1.87Å $d_{Shannon} = 1.86Å$

**P(1) Tetrahedron**

| P(1) | O(1) | O(1) | O(1) | O(1) |
|---|---|---|---|---|
| O(1) | **1.532(2)** | 2.523(2) | 2.523(2) | 2.458(3) |
| | **1.577(4)** | 2.596(2) | 2.596(2) | 2.528(2) |
| O(1) | 110.9(1) | **1.532(2)** | 2.458(3) | 2.523(2) |
| | 110.8(1) | **1.577(4)** | 2.528(2) | 2.596(2) |
| O(1) | 110.9(1) | 106.7(1) | **1.532(2)** | 2.523(2) |
| | 110.8(1) | 106.8(4) | **1.577(4)** | 2.596(2) |
| O(1) | 106.7(1) | 110.9(1) | 110.9(1) | **1.532(2)** |
| | 106.8(4) | 110.8(1) | 110.8(1) | **1.577(4)** |

**<P-O> = 1.53Å,** 1.58Å $d_{Shannon} = 1.52Å$

**P(2) Tetrahedron**

| P(2) | O(2) | O(2) | O(2) | O(2) |
|---|---|---|---|---|
| O(2) | **1.531(2)** | 2.518(4) | 2.453(2) | 2.527(1) |
| | **1.488(5)** | 2.451(3) | 2.369(3) | 2.471(1) |
| O(2) | 110.7(1) | **1.531(2)** | 2.527(1) | 2.453(2) |
| | 110.9(2) | **1.488(5)** | 2.471(1) | 2.369(3) |
| O(2) | 106.5(1) | 111.3(1) | **1.531(2)** | 2.518(4) |
| | 105.4(3) | 112.2(2) | **1.488(5)** | 2.451(3) |
| O(2) | 111.3(1) | 106.5(1) | 110.7(1) | **1.531(2)** |
| | 112.2(2) | 105.4(3) | 110.9(2) | **1.488(5)** |

**<P-O> = 1.53Å,** 1.49Å $d_{Shannon} = 1.52Å$

**TABLE 9**—*Continued*

| P(3) Tetrahedron | | | | |
|---|---|---|---|---|
| **P(3)** | **O(3)** | **O(3)** | **O(4)** | **O(4)** |
| **O(3)** | **1.530(1)** | 2.518(3) | 2.527(5) | 2.447(3) |
| | **1.534(2)** | 2.484(1) | 2.567(5) | 2.451(1) |
| **O(3)** | 110.8(1) | **1.530(1)** | 2.447(3) | 2.527(5) |
| | 108.2(1) | **1.534(2)** | 2.451(1) | 2.567(5) |
| **O(4)** | 111.4(1) | 106.2(1) | **1.530(1)** | 2.519(3) |
| | 113.7(2) | 106.1(1) | **1.433(2)** | 2.500(3) |
| **O(4)** | 106.2(1) | 111.4(1) | 110.9(1) | **1.530(1)** |
| | 106.1(1) | 113.7(2) | 109.2(2) | **1.433(2)** |

**<P-O> = 1.53Å,** 1.48Å $d_{Shannon}$ = *1.52Å*

| Polyèdre Na(1) CN 7 | | |
|---|---|---|
| Na(1)-O(1) | 2×2.391(3) | 2×2.302(4) |
| Na(1)-F(2) | 2×2.433(3) | 2×2.399(4) |
| Na(1)-F(1) | 2.475(3) | 2.496(8) |
| Na(1)-O(3) | 2×2.490(4) | 2×2.575(4) |
| **<Na(1)-O, F>** | **2.44** | **2.43** |

| Polyèdre Na(2) CN 7 | | |
|---|---|---|
| Na(2)-O(2) | 2×2.409(4) | 2×2.346(4) |
| Na(2)-F(2) | 2×2.433(3) | 2×2.461(5) |
| Na(2)-O(4) | 2×2.437(4) | 2×2.451(4) |
| Na(2)-F(1) | 2.477(3) | 2.448(5) |
| **<Na(2)-O, F>** | **2.43** | **2.42** |

| Polyèdre Na(3) CN 7 | | |
|---|---|---|
| Na(3)-O(3) | 2×2.385(4) | 2×2.237(7) |
| Na(3)-F(2) | 2×2.443(3) | 2×2.51(1) |
| Na(3)-F(1) | 2.475(3) | 2.50(3) |
| Na(3)-O(2) | 2×2.205(6) | 2×2.75(3) |
| **<Na(3)-O, F>** | **2.45** | **2.50** |

| Polyèdre Na(4) CN 7 | | |
|---|---|---|
| Na(4)-O(4) | 2×2.425(5) | 2×2.326(4) |
| Na(4)-F(2) | 2×2.441(3) | 2×2.427(4) |
| Na(4)-O(1) | 2×2.449(4) | 2×2.569(4) |
| Na(4)-F(1) | 2.495(4) | 2.576(7) |
| **<Na(4)-O, F>** | **2.43** | **2.42** |

| Polyèdre Na(5) CN 6 | | |
|---|---|---|
| Na(5)-F(2) | 2×2.340(7) | 2×2.277(6) |
| Na(5)-O(1) | 2×2.463(5) | 2×2.462(5) |
| Na(5)-O(1) | 2×2.478(6) | 2×2.486(5) |
| **<Na(5)-O, F>** | **2.43** | **2.41** |

| Polyèdre Na(6) CN 6,7 | | |
|---|---|---|
| Na(6)-F(2) | 2×2.288(5) | 2×2.302(2) |
| Na(6)-O(2) | 2×2.430(9) | 2×2.399(1) |
| Na(6)-O(2) | 2×2.59(1) | |
| Na(6)-F(1) | | 2.52(4) |
| Na(6)-O(4) | | 2×2.71(3) |
| **<Na(6)-O, F>** | **2.44** | **2.48** |

**TABLE 9**—*Continued*

| Polyèdre Na(7) CN 6 | | |
|---|---|---|
| Na(7)-F(2) | 2×2.281(3) | 2×2.351(3) |
| Na(7)-O(4) | 2×2.492(7) | 2×2.485(4) |
| Na(7)-O(3) | 2×2.557(8) | 2×2.496(4) |
| **<Na(7)-O, F>** | **2.44** | **2.44** |

| Polyèdre Na(8) CN 6, 7 | | |
|---|---|---|
| Na(8)-F(2) | 2×2.223(7) | 2×2.400(5) |
| Na(8)-O(3) | 2×2.48(2) | 2×2.293(5) |
| Na(8)-O(4) | 2×2.60(2) | |
| Na(8)-F(1) | | 2.502(8) |
| Na(8)-O(1) | | 2×2.606(5) |
| **<Na(8)-O, F>** | **2.43** | **2.44** |

basis of the $\beta_2$ form (isostructural with $M = V^{3+}$), which was described in the new space group. Taking into account the volume relation between the two forms ($V\gamma = 2V\beta_2$), the number of atoms per unit cell in the low temperature form is doubled. The expected number of Na atoms is 24, but the description of the two sodium sites (8*i*) in $\beta_2$ form to the *Pbam* space group generates eight sites (4*h*, 4*g*), corresponding to 32 atoms per unit cell. So, the site occupation factors are refined and lead to a value close to zero for two Na sites (at $z = 0$ and $z = 1/2$). The refinement is then carried out with only six sites for the Na atoms, and their associated sof converging around 0.5 (fully occupied sites) are fixed at the end. The conventional reliability factors take the following values: $R_p = 9.74\%$, $R\omega_p = 9.48\%$ and $\chi^2 = 2.68$ for 68 re-

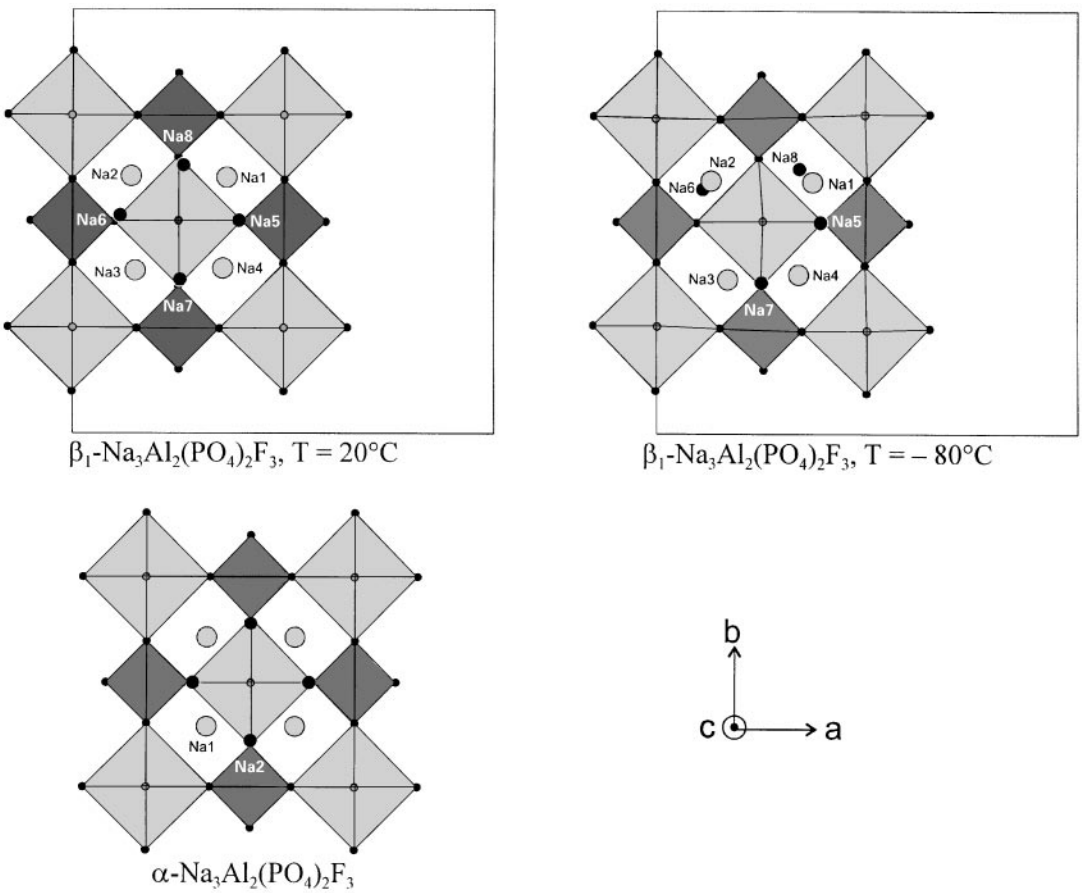


**FIG. 7.** Projections along the *c* axis ($-0.4 < z < 0.1$) for the different modifications of $Na_3Al_2(PO_4)_2F_3$ (all Na atoms are at $z = 0$; atom label as in Tables 8 and 10).

**TABLE 10**
**Atomic Parameters and Equivalent Isotropic Displacement Parameters (Å²) for $\beta_2$-$Na_3V_2(PO_4)_2F_3$**

| Atoms | Site | sof | $x$ | $y$ | $z$ | $B_{eq}$ |
|---|---|---|---|---|---|---|
| Na(1) | 8*i* | 0.5 | 0.5234(3) | 0.2299(5) | 0 | 2.93(7) |
| Na(2) | 8*i* | 0.25[a] | 0.803(1) | 0.0512(8) | 0 | 8.3(3) |
| V | 8*j* | 0.5 | 0.24783(6) | 0.24783(6) | 0.18845(4) | 0.578(2) |
| P(1) | 4*d* | 0.25 | 0 | $\frac{1}{2}$ | $\frac{1}{4}$ | 0.88(4) |
| P(2) | 4*e* | 0.25 | 0 | 0 | 0.2553(1) | 0.08(3) |
| O(1) | 16*k* | 1 | 0.0969(4) | 0.4059(4) | 0.1629(5) | 1.02(8) |
| O(2) | 8*j* | 0.5 | 0.0947(4) | 0.0947(4) | 0.1682(5) | 0.87(7) |
| O(3) | 8*j* | 0.5 | 0.4031(4) | 0.4031(4) | 0.1605(5) | 0.79(8) |
| F(1) | 4*f* | 0.25 | 0.2476(3) | 0.2476(3) | 0 | 0.59(1) |
| F(2) | 8*j* | 0.5 | 0.2466(2) | 0.2466(2) | 0.3642(2) | 0.96(1) |

[a] Fixed.

fined parameters. The main results of this refinement are summarized in Table 13 whereas the atomic positions are listed in Table 11. Conditions of data collection for $\gamma$-$Na_3Fe_2(PO_4)_2F_3$ are found in Table 12 and some interatomic distances are presented in Table 14.

Once more, the main difference between the two varieties $\gamma$ and $\beta_2$ lies in the positions adopted by the Na atoms, but also in the deformation of the polyhedra of the host matrix. Figure 9 allows a fast comparison between the two forms. It gives an account of the very clear deformation of the host network $[Fe_2(PO_4)_2F_3]^{3-}$ which probably makes the important motions (around 0.7 Å) of the $Na^+$ cations accompanying the $\gamma \leftrightarrow \beta_2$ transition easier.

## STRUCTURAL DESCRIPTION AND CORRELATIONS

Figure 10 (23) represents a perspective view of the three-dimensional network exhibited by the family of $Na_3M_2(PO_4)_2F_3$. The structural unit is built up from $[M_2^{III}O_8F_3] \equiv [M_2^{III}X_{11}]$ bioctahedra and $[PO_4]$ tetrahedra. The connection between the two octahedra is enabled by a bridging fluorine apex. Each bioctahedron shares all its eight oxygen vertices with tetrahedra. From such a linkage, the resulting channels run along *a* and *b* axes while their intersections build rather large cavities in which $Na^+$ cations are located. The remaining free fluorine vertices point toward the center of these cavities. The longer Al–*X* and V–*X* distances ($X$ = O, F) are associated with the shared anions; whereas distances with terminal fluorine atoms (F(2) in each structural type) are obviously shorter. As shown previously, the main difference between each structural form of the family is the localization of the $Na^+$ cations with statistical distribution in the anionic framework cavities as shown in Figs. 7 and 9.

The three-dimensional framework of $Na_3[M_2(PO_4)_2F_3]$ phases has been also encountered in the $Al(H_2O)_4[Ca_2(SO_4)_2F_2Cl]$ mineral (Vlodavetsite (24)) (Fig. 11). The main difference is the presence of $Al^{3+}$ cations in neighboring octahedral $[AlF_2(H_2O)_4]$ which are connected by the two *trans* F vertices to two bioctahedral dimers $[Ca_2O_8F_2Cl]$ along *c* and form chains with the Al–Ca–Ca sequence. The presence of a $Cl^-$ anion shared between the two $Ca^{2+}$ octahedra of the dimer extends the cavity and allows the insertion of an $Al^{3+}$ cation with four water molecules. The distance between two F vertices of successive dimers is 3.5 Å (Al–F = 1.75 Å), whereas in the $Na_3Al_2(PO_4)_2F_3$ the same distance drops down to $\approx 3$ Å.

The three-dimensional network can also be described as the stacking of staggered layers in the (*a*, *b*) plane of the $[M(PO_4)F_2]$ formula. These layers are linked via F vertices to the octahedra of an adjacent layer along *c* to form

**TABLE 11**
**Main Interatomic Distances (Å) and Angles (°) for $\beta_2$-$Na_3V_2(PO_4)_2F_3$**

V Octahedron

| V | $F(2)^{terminal}$ | O(2) | O(1) | O(1) | O(3) | F(1) |
|---|---|---|---|---|---|---|
| $F(2)^{terminal}$ | **1.881(2)** | 2.860(2) | 2.925(4) | 2.925(4) | 2.960(1) | 3.898(2) |
| O(2) | 95.8(2) | **1.972(4)** | 2.817(4) | 2.817(4) | 3.947(2) | 2.659(4) |
| O(1) | 97.9(2) | 90.4(2) | **1.996(4)** | 3.954(2) | 2.770(4) | 2.637(3) |
| O(1) | 97.9(2) | 90.4(2) | 164.0(2) | **1.996(4)** | 2.009(4) | 2.637(3) |
| O(3) | 99.0(2) | 165.1(2) | 87.5(1) | 87.5(1) | **2.009(4)** | 2.629(4) |
| F(1) | 179.4(1) | 83.6(2) | 82.1(2) | 82.1(2) | 81.5(2) | **2.017(1)** |

⟨V–O, F⟩ 1.98 Å, $d_{Shannon}$ 1.98 Å

P(1) Tetrahedron

| P(1) | O(1) | O(1) | O(1) | O(1) |
|---|---|---|---|---|
| O(1) | **1.537(4)** | 2.542(4) | 2.443(4) | 2.542(4) |
| O(1) | 111.6(2) | **1.537(4)** | 2.542(4) | 2.542(4) |
| O(1) | 105.3(3) | 111.6(2) | **1.537(4)** | 2.542(4) |
| O(1) | 111.6(2) | 105.3(3) | 111.6(2) | **1.537(4)** |

⟨P–O⟩ 1.54 Å, $d_{Shannon}$ 1.52 Å

P(2) Tetrahedron

| P(2) | O(2) | O(2) | O(3) | O(3) |
|---|---|---|---|---|
| O(2) | **1.528(5)** | 2.422(2) | 2.523(1) | 2.523(1) |
| O(2) | 104.8(3) | **1.528(5)** | 2.523(1) | 2.523(1) |
| O(3) | 111.0(2) | 111.0(2) | **1.533(4)** | 2.479(3) |
| O(3) | 111.0(2) | 111.0(2) | 108.0(3) | **1.533(4)** |

⟨P–O⟩ 1.53 Å

| Na(1) Polyhedron CN 7 | | Na(2) Polyhedron CN 7 | |
|---|---|---|---|
| Na(1)–O(1) | 2 × 2.370(4) | Na(2)–F(2) | 2 × 2.391(8) |
| Na(1)–F(2) | 2 × 2.498(3) | Na(2)–O(2) | 2 × 2.418(3) |
| Na(1)–F(1) | 2.500(4) | Na(2)–F(1) | 2.74(1) |
| Na(1)–O(3) | 2 × 2.568(5) | Na(2)–O(1) | 2 × 2.898(8) |
| **⟨Na–O, F⟩** | **2.48** | **⟨Na–O, F⟩** | **2.59** |

$d_{Shannon}$ 2.45 Å

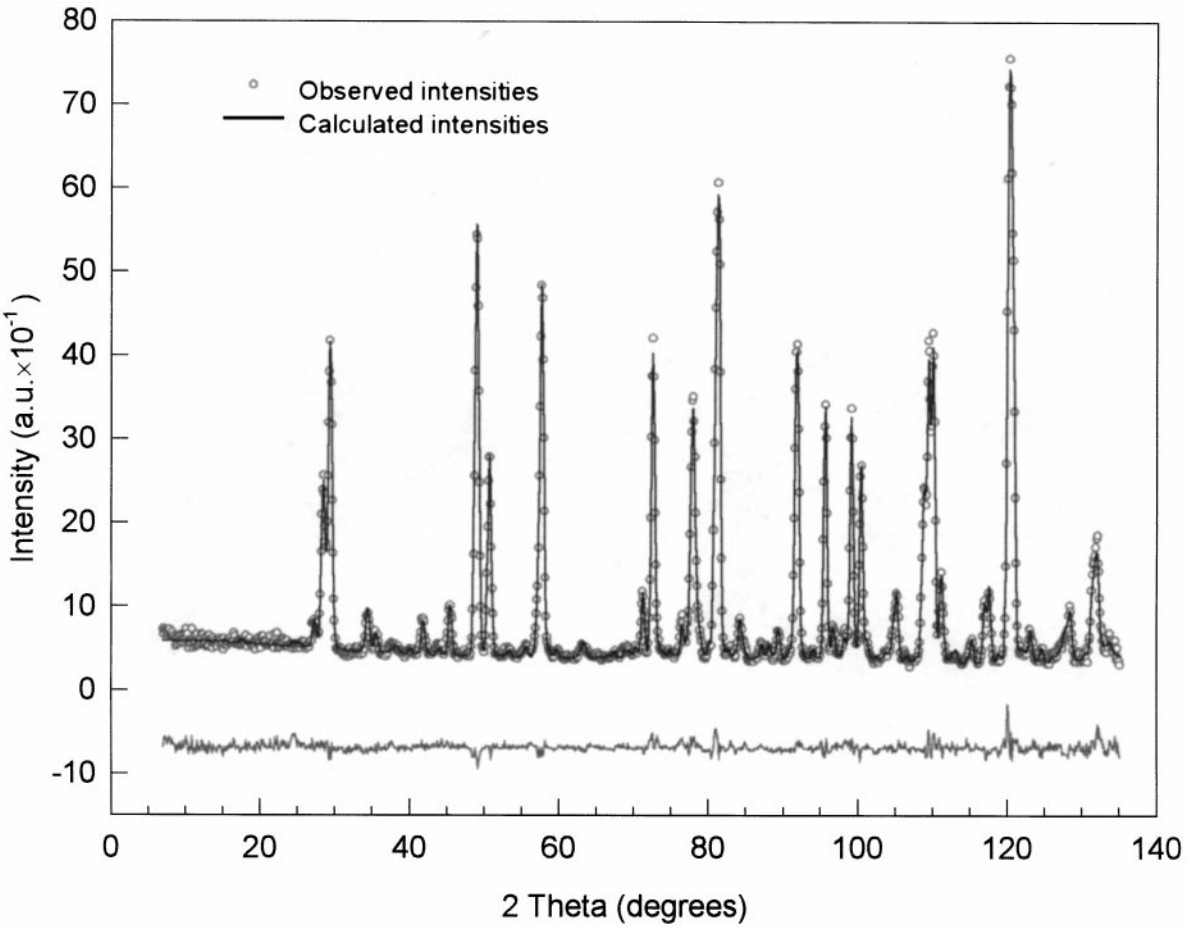


**FIG. 8.** Neutron diffraction pattern of $\gamma$-$Na_3Fe_2(PO_4)_2F_3$ at $-190°C$.

tunnels. As noticed by Yakubovich *et al.* (7), this structure is closely related to the structure of $Na_2TiSiO_5$, $Li_2TiSiO_5$ (25); instead of a three-dimensional network, only $[TiSiO_5]^{2-}$ layers are encountered in the (*a*, *b*) plane; their cohesion is made possible by the presence of $Li^+$ cations in the Van der Waals void. In these compounds (Figure 12), $Ti^{4+}$ cations are in 5-coordination (tetragonal pyramid, $Ti–O_{av} = 1.92$ Å) because the sixth Ti–O bond ($\approx 2.70$ Å) is longer. Nevertheless, with a pseudo-$Ti^{4+}$ octahedral coordination, the structure can be viewed as linear chains along the *c* direction linked by $SiO_4$ tetrahedra to form a three-dimensional network slightly different from the one of the $Na_3M_2(PO_4)_2F_3$ family. Indeed, two successive layers are deduced thanks to a mirror in the (*a*, *b*) plane in $Na_3M_2(PO_4)_2F_3$ whereas in $Na_2TiSiO_5$ they remain identical. The same topology of layers have also been encountered in $ASbPO_4F.xH_2O$ ($A = NH_4$, Na; $x = 0$, 1, 1.5, and 3) (26), $VOPO_4(H_2O)_2$ (27), and $VOPO_4$–0.5 piperazin (28). In the Sb series, $Sb^{3+}$ adopts the same 5-coordination as $Ti^{4+}$ in $Na_2TiSiO_5$ but the layer is larger because the tetragonal pyramids are stacked on either side of the tetrahedra. The stacking of the layers and the interlayer distance depends on the cations and the number of intercalated water molecules.

## MAGNETIC STUDY

Three compounds including paramagnetic cations have been studied ($V^{3+}$, $Cr^{3+}$, $Fe^{3+}$). This study presents the main results concerning the susceptibility measurements. Figure 13 shows the inverse magnetic susceptibility temperature dependence. All these curves are characteristic of an antiferromagnetic behavior, except for the glassy iron compound. Magnetic associated data are listed in Table 15. Experimental and calculated Curie molar constants match, except for the crystallized iron compound for which further higher temperature data would be necessary. The asymptotic Curie temperatures ($\theta_p$) indicate the presence of strong antiferromagnetic interactions which are expected inside the bioctahedral dimer $[M_2O_8F_3]$. Moreover, the $|\theta_p/T_N|$ ratio greater than unity suggests the presence of magnetic frustration.

**TABLE 12**
**Conditions of Data Collection and Main Refinement Results for $\gamma$-$Na_3Fe_2(PO_4)_2F_3$ at $-190^\circ C$ (Paramagnetic State)**

| | |
|---|---|
| Angular range ($2\theta$) | 2°–138.9° |
| Step ($2\theta$) | 0.1° |
| Refinement program | FULLPROF |
| Wavelength | 2.597 Å |
| Background | Manually selected |
| Zero point ($2\theta$) | 1.085 (6) |
| ETA | 0.085 (7) |
| FWHM parameters | $U_1 = 0.16(1)$ $V_1 = -0.37(2)$ $W_1 = 0.47(1)$ |
| Asymmetry parameters | 0.064 (6) |
| Number of refined parameters | 68 (parameters concerning impurities fixed) |
| Space group | *Pbam* (No. 55) |
| Unit cell parameters (Å) | $a''' = 12.756(1)$, $b''' = 12.803(1)$, $c''' = 10.602(1)$ |
| Scale factor | 0.024 (1) |
| Number of reflections | 367 |
| Reliability[a] | $R_B = 4.56$ $R_f = 5.37$ |
| Percentage of contribution | 93.0% |
| Conventional reliability factors[a] | $R_p = 9.74\%$, $R\omega_p = 9.48\%$, $\chi^2 = 2.12$ |

[a] Following FULLPROF refinement program definition.

From Fig. 7 (or 10), it can be seen that the long range magnetic order between bioctahedra involves a magnetic coupling by super-superexchange (SSE) via the $PO_4$ tetra-hedra. Indeed, the paramagnetic neighboring is as follows: the nearest neighbor is found in the dimer at $d_1$ close to 4.0 Å (superexchange angle near 179°), then the next nearest neighbors are four $M^{3+}$ at $d_2 \approx 4.7$ Å (SSE angle near 113°), and finally four other $M^{3+}$ at $d_3 \approx 6.4$ Å (SSE angle near 173°). So, the minimum observed on the $\chi^{-1} = f(T)$ graph does not match with the Néel temperature but rather with the beginning of the magnetic ordering within the dimers. For the crystallized compound with $M = Fe^{3+}$, the $T_N$ temperature (3D order) determined by Mössbauer studies (29) of hyperfine field evolution versus temperature—$T_N = 62(2)$ K—is actually far from the very weak minimum of 10(10) K given in Table 15.

This leads to an interesting study about the importance of super-superexchange in such materials. The detailed magnetic study of the $M = Fe^{3+}$ compound will be the subject of a future paper (29).

**TABLE 13**
**Atomic Coordinates and Isotropic Atomic Displacement Parameters $B_{eq}$ for $\gamma$-$Na_3Fe_2(PO_4)_2F_3$ at $-190^\circ C$**

| Atoms | Site | sof | $x$ | $y$ | $z$ | $B_{iso}$[a] (Å)$^2$ |
|---|---|---|---|---|---|---|
| Na(1) | 4*g* | 0.5 | 0.112(4) | 0.411(3) | 0 | 1.20 |
| Na(2) | 4*h* | 0.5 | 0.116(3) | 0.131(3) | $\frac{1}{2}$ | 1.20 |
| Na(3) | 4*h* | 0.5 | 0.407(4) | 0.360(3) | $\frac{1}{2}$ | 1.20 |
| Na(4) | 4*g* | 0.5 | 0.385(4) | 0.386(3) | 0 | 1.20 |
| Na(5) | 4*h* | 0.5 | 0.103(4) | 0.362(4) | $\frac{1}{2}$ | 1.20 |
| Na(6) | 4*g* | 0.5 | 0.338(3) | 0.615(4) | 0 | 1.20 |
| Fe(1) | 8*i* | 1 | 0.002(1) | 0.249(1) | 0.1842(7) | 0.15 |
| Fe(2) | 8*i* | 1 | 0.249(2) | −0.047(8) | 0.3068(6) | 0.15 |
| P(1) | 8*i* | 1 | 0.240(2) | 0.252(1) | 0.242(1) | 0.15 |
| P(2) | 4*e* | 0.5 | 0 | 0 | 0.237(3) | 0.15 |
| P(3) | 4*f* | 0.5 | 0 | $\frac{1}{2}$ | 0.245(4) | 0.15 |
| O(1) | 8*i* | 1 | 0.243(2) | 0.350(1) | 0.347(2) | 0.60 |
| O(2) | 8*i* | 1 | 0.154(1) | 0.257(1) | 0.849(2) | 0.60 |
| O(3) | 8*i* | 1 | 0.254(2) | 0.642(1) | 0.322(1) | 0.60 |
| O(4) | 8*i* | 1 | 0.350(1) | 0.266(1) | 0.173(2) | 0.60 |
| O(5) | 8*i* | 1 | 0.012(2) | 0.089(2) | 0.164(2) | 0.60 |
| O(6) | 8*i* | 1 | 0.404(2) | −0.013(1) | 0.329(2) | 0.60 |
| O(7) | 8*i* | 1 | −0.011(1) | 0.414(2) | 0.159(2) | 0.60 |
| O(8) | 8*i* | 1 | 0.095(2) | −0.005(1) | 0.335(2) | 0.60 |
| F(1) | 4*g* | 0.5 | −0.003(2) | 0.251(4) | 0 | 0.90 |
| F(2) | 4*h* | 0.5 | 0.245(4) | −0.002(2) | $\frac{1}{2}$ | 0.90 |
| F(3) | 8*i* | 1 | 0.006(2) | 0.255(2) | 0.373(1) | 0.90 |
| F(4) | 8*i* | 1 | 0.247(3) | −0.017(1) | 0.136(1) | 0.90 |

[a] The isotropic ADPs were fixed following the nature of the associated atom.

**TABLE 14**
**Main Interatomic Distances in $\gamma$-$Na_3Fe_2(PO_4)_2F_3$**

| Fe(1) Octahedron | | Fe(2) Octahedron | |
|---|---|---|---|
| O(4) | 1.95(1) | $F(4)^{terminal}$ | 1.81(1) |
| F(1) | 1.95(1) | O(3) | 1.89(1) |
| O(2) | 1.97(1) | O(1) | 1.90(1) |
| $F(3)^{terminal}$ | 2.03(1) | O(8) | 1.93(1) |
| O(7) | 2.11(1) | F(2) | 2.05(1) |
| O(5) | 2.11(1) | O(6) | 2.07(1) |
| ⟨Fe(1)–O,F⟩ = 2.02 Å | | ⟨Fe(2)–O,F⟩ = 1.94 Å | |

| P(1) Tetrahedron | | P(2) Tetrahedron | | P(3) Tetrahedron | |
|---|---|---|---|---|---|
| O(2) | 1.49(1) | O(5) | 1.37(1) | O(7) | 1.46(1) |
| O(4) | 1.55(1) | O(5) | 1.37(1) | O(7) | 1.46(1) |
| O(3) | 1.63(1) | O(8) | 1.60(1) | O(6) | 1.48(1) |
| O(1) | 1.70(1) | O(8) | 1.60(1) | O(6) | 1.48(1) |
| ⟨P(1)–O⟩ = 1.59 Å | | ⟨P(2)–O⟩ = 1.49 Å | | ⟨P(3)–O⟩ = 1.47 Å | |

Mean distances involving $Na^+$ (sevenfold coordination)

⟨Na(1)–O, F⟩ = 2.47 Å ⟨Na(2)–O, F⟩ = 2.50 Å ⟨Na(4)–O, F⟩ = 2.52 Å
⟨Na(5)–O, F⟩ = 2.45 Å ⟨Na(6)–O, F⟩ = 2.39 Å ⟨Na(7)–O, F⟩ = 2.54 Å

## CONCLUSION

The compounds $Na_3M_2(PO_4)_3F_3$ set up an interesting fluorophosphate family. The present study allows us to go further into the knowledge of these phases in the fields of chemistry, thermal and magnetic behavior, and finally crystal structures.

From a chemical point of view the family was extended to the compounds with $M =$ Al, Ga, V, and Cr (already reported by Nagorniy *et al.* (30)). These phases can be prepared by solid state synthesis (Al, Cr, Fe), by hydrothermal route (Al, V, Fe, Ga), or by recrystallization of glasses

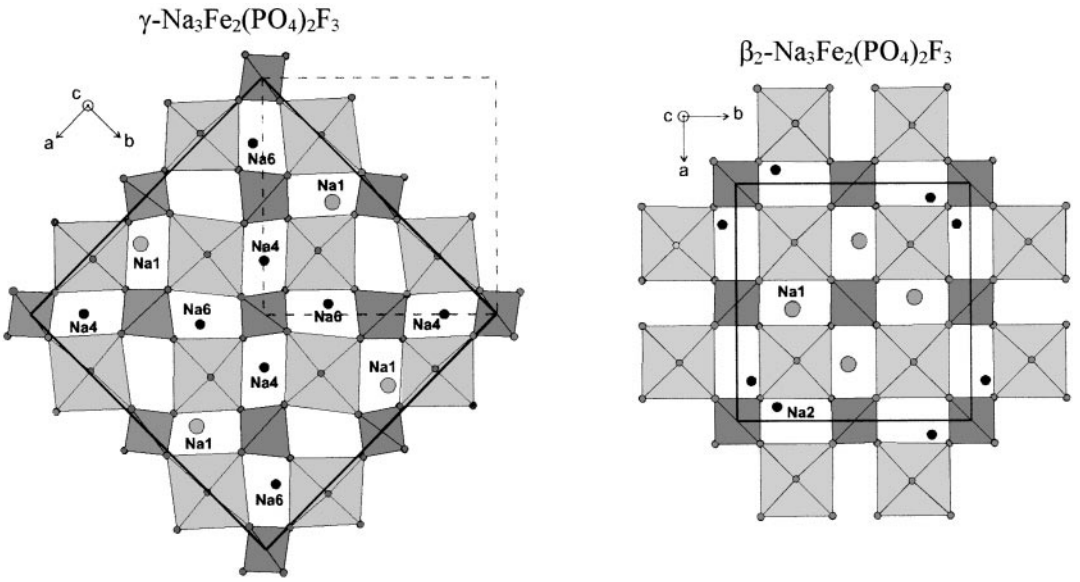


**FIG. 9.** Projection along $c$ axis ( $-0.5 \leq z \leq 0$) of two varieties of $Na_3Fe_2(PO_4)_2F_3$: $\gamma$ (on the left) and $\beta_2$ (on the right) (broken lines represent the $\beta_2$ unit cell in relation to the $\gamma$ one; all the $Na^+$ cations are at level $z = 0$).

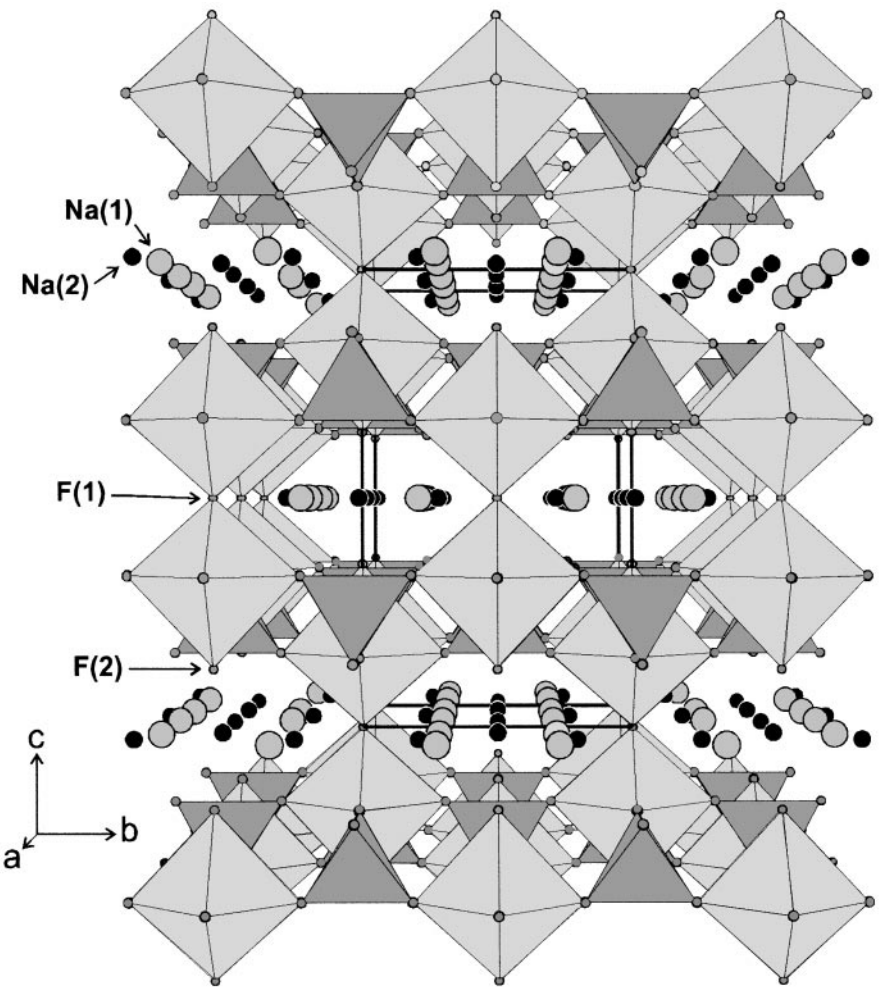


**FIG. 10.** Perspective view along the $a$ axis of $\alpha$-$Na_3Al_2(PO_4)_2F_3$ three-dimensional network (the sodium sites are represented fully occupied).

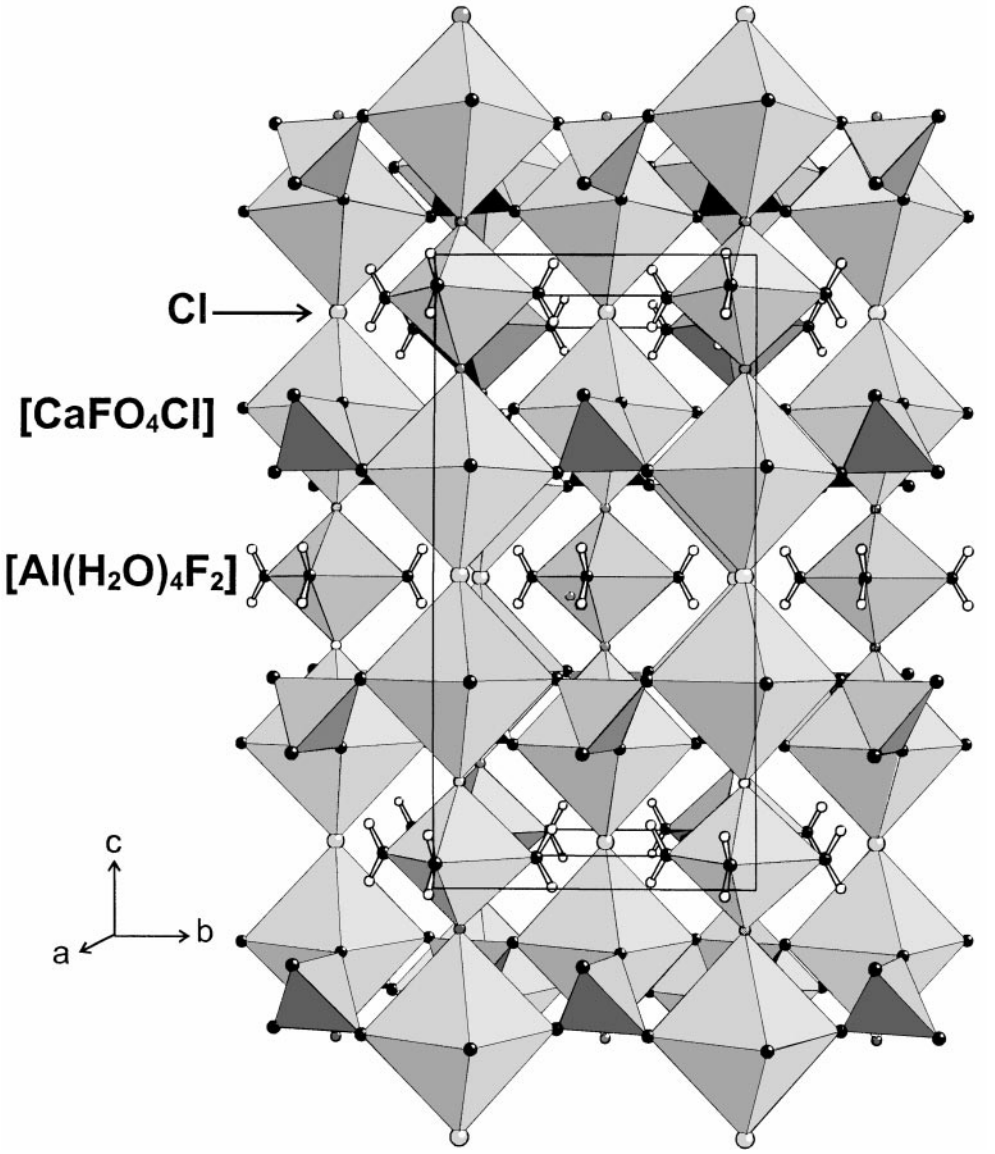


**FIG. 11.** Perspective view of the three-dimensional network of $Al(H_2O)_4[Ca_2(SO_4)_2F_2Cl]$ (the bridging $Cl^-$ anion increases the space of the cavities and allows the insertion of $Al^{3+}$ cations with four molecules of water).

(Al, Fe). All the compounds are stable and we have never observed any OH/F substitution during the hydrothermal syntheses.

From a thermal point of view, three modification havebeen evidenced: namely the $\gamma$, $\beta$, and $\alpha$ forms (from low to high temperature). The structural transition temperatures were highlighted by various experimental techniques including as DSC, X-ray thermodiffractometry, or Mössbauer spectrometry (Fe). At room temperature all the compounds crystallize in the $\beta$ form. The transition temperatures $\gamma \leftrightarrow \beta_{1\,or\,2}$ for $M$ = Al and V and $\beta \leftrightarrow \alpha$ for $M$ = Ga are not determined yet.

From a structural point of view the structure of each polymorph has been determined ($\alpha$ (Al), $\beta_1$ (Al), $\beta$ (V), and $\gamma$ (Fe)). The $\alpha$ form is the same as reported by Yakubovitch *et al.* (8, 20) for the Fe and Al compounds despite the fact that only two sites are required to describe the statistical distribution of the $Na^+$ ions in the cavities. The observed superstructure for the $\beta_1$ form ($V_{\beta 1} \approx 4V_\alpha$) is mainly due to a displacement of the sodium atoms in the cavities (about 0.2–0.3 Å). The $\beta_2$ form, studied on the vanadium compound, is isotypic to the structure of the $Na_3Fe_2(PO_4)_2(OH)_2F$ previously reported by Yakubovitch *et al.* (7). Once more, the superstructure comes from a different distribution of the sodium atoms inside the cavities ($V_{\beta 2} \approx 2V_\alpha$). Finally, the structure of the $\gamma$ form was studied on the Fe compound by powder neutron diffraction ($\lambda$ = 2.60 Å). The $\gamma$ form correponds to a slight orthrhombic distortion of the

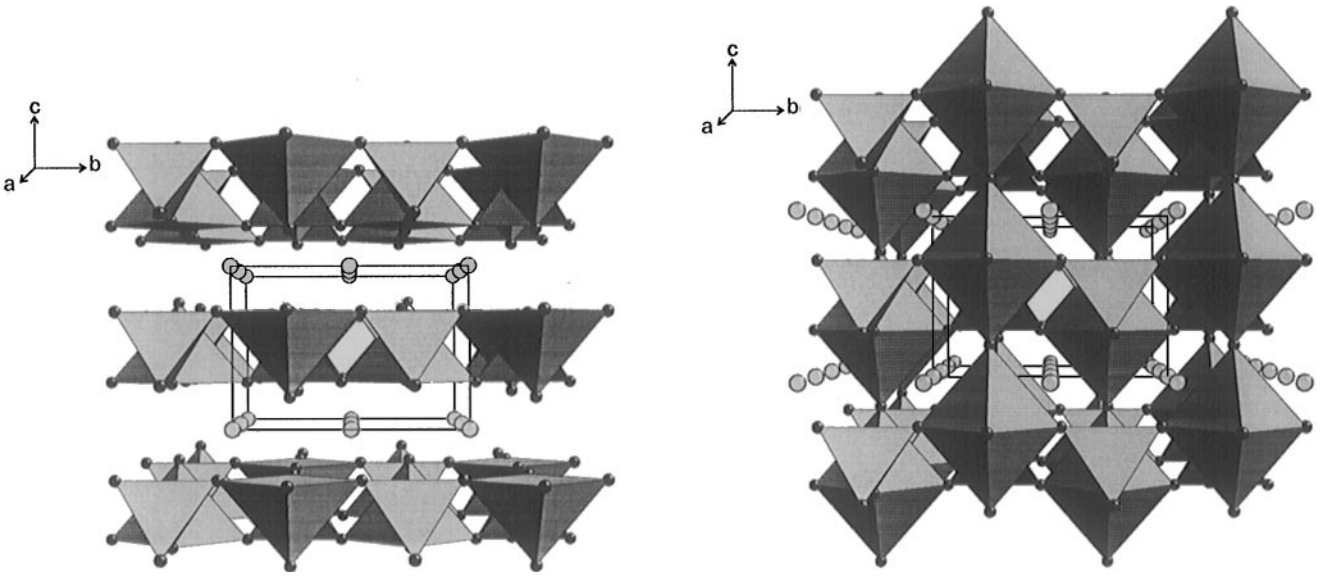


**FIG. 12.** Perspective view of the $Li_2TiSiO_5$ structure: the two-dimensional network (on the left) and the three-dimensional network based on the pseudo coordination [6] for the Ti species (on the right).

tetragonal $\beta_1$ cell ($V_\gamma \approx 4V_\alpha$). This structure gives rise to a new repartition of the sodium atoms but also to a slight distortion of the polyhedra framework.

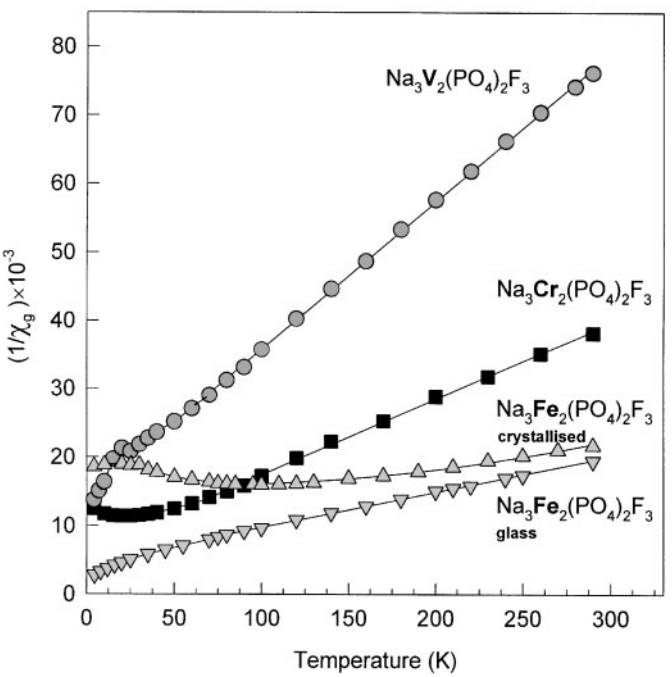


**FIG. 13.** Thermal variation of the inverse magnetic susceptibility for the compounds $Na_3M_2(PO_4)_2F_3$.

From a magnetic point of view, the phases with $M = V$, Cr, and Fe behave as antiferromagnets. According to th peculiar structure of this family, i.e., a three-dimensional network of bioctahedra $M_2O_8F_3$ linked together by $PO_4$ tetrahedra, the long range magnetic order is set up by SSE magnetic couplings. The determination of the magnetic structure (29) has shown the important part of the SSE couplings in this framework.

The observed phase transitions originate from the different distributions of the $Na^+$ ions in the cavities offered by the 3D network $[M_2(PO_4)_2F_3]$. Ionic conductivity measurements (31) have been performed on the Al compound ($\alpha$-form) in the temperature range 20–650°C. The ionic mobility of $Na^+$ remains weak while the conductivity has a bidimensional character ($E_0 = 0.8$ eV).

Finally, taking into account the structural relationship between the family $Na_3M_2(PO_4)_2F_3$ and the mineral vlodavetsite $(Al(H_2O)_4)[Ca_2(SO_4)_2F_2Cl]$, the synthesis of new materials could be attempted for various purposes.

**TABLE 15**
**Magnetic Data for $Na_3M_2(PO_4)_2F_3$, $M = Fe^{3+}$, $V^{3+}$, $Cr^{3+}$**

| Cation | Interactions | $T_N$ (K) | $\theta_p$ (K) | $\lvert\theta_p/T_N\rvert$ | $C_M$ exp[a] | $C_M$ theo[a] |
|---|---|---|---|---|---|---|
| $V^{3+}$ | AF | 25(5) | − 69(7) | 2.8 | 0.98 | 1.00 |
| $Cr^{3+}$ | AF | 22(5) | − 59(8) | 2.7 | 1.88 | 1.87 |
| $Fe^{3+}$ | AF | 100(10) | − 239(15) | 2.4 | 4.97 | 4.38 |
| $Fe^{3+}$[b] | — | — | − 88(3) | — | 4.13 | 4.38 |

[a] Calculated for one $M^{3+}$ ion.
[b] Glassy state.

## ACKNOWLEDGMENTS

The authors gratefully acknowledge Profs. M. Leblanc (Laboratoire des Fluorures, Le Mans) and M. Evain (IMN Nantes) for their help in the RX data collection of the crystals. Thanks are also due to Dr. P. Chevallier (IMN Nantes) for thermodiffractometry at low temperature on D5000. Finally, we thank Dr. J.-M. Grenèche (Laboratoire de Physique de l'Etat Condensé, Le Mans) for Mössbauer experiments and critical reading, Prof. I. Richard (Université du Maine) for a very careful final reading and the two reviewers for their relevant and constructive suggestions.

## REFERENCES

1. J. Arlt, M. Jansen, H. Klassen, G. Schimmel, and G. Heymer, *Z. Anorg. Allg. Chem.* **547,** 179 (1987).
2. P. G. Naornyi, A. A. Kapshuk, Z. I. Kornienko, V. V. Mitkevich, and S. M. Tretiak, *Zh. Neorg. Khim.* **35,** 839 (1990).
3. D. M. Poojary, A. Clearfield, V. A. Timofeeva, and S. E. Sigaryov, *Solid State Ionics* **73,** 75 (1994).
4. O. L. Slovokhotova, G. D. Ilyushin, N. S. Triodina, O. K. Mel'nikov, L. N. Dem'yanets, R. G. Gerr, and V. G. Tsirel'son, **32,** 103 (1991).
5. N. S. Slobodyanik P. G. Nagornyi, Z. I. Kornienko, and A. A. Kapshuk, *Zh. Neorg. Khim.* **36,** 1390 (1991).
6. E. L. Belokoneva, O. V. Yakubovich, V. G. Tsirelson, and V. S. Urusov, *Izv. Akad. Nauk Neor. Mat.* **26,** 295 (1990).
7. O. V. Yakubovich, M. A. Simonov, and O. K. Mel'nikov, *Kristallografiya* **29,** 484 (1984).
8. O. V. Yakubovich and O. K. Mel'nikov, *Doklady Akad. Nauk* **342**(5), 615 (1995).
9. J.-M. Le Meins, Thesis, chapter I, University of Le Mans, 1998.
10. "International Tables for X-ray Crystallography," Vol. IV. Kynoch Press, Birmingham, 1974.
11. G. M. Sheldrick, Shelxs-86, *in* "Crystallographic Computing 3" (G. M. Sheldrick, C. Kruger, and R. Goddard, Eds.) p. 175. Oxford Univ. Press, London/New York, 1985.
12. G. M. Sheldrick, "SHELXL-93, A Program for Crystal Structure Determination," University of Göttingen, Germany, 1993.
13. V. Petricek and M. Dusek, "JANA-96, Crystallographic Computing System." Institute of Physics, Praha, 1996.
14. J. Rodriguez-Carvajal, "FULLPROF, Profil Matching Tool/Rietveld Analysis of Neutron or X-Ray Powder Diffraction Data." Institut Laue-Langevin, 1997.
15. J. J. Videau, Thesis, University of Bordeaux I, 1979.
16. J. C. Warf, W. D. Cline, and R. D. Tevebaugh, *Anal. Chem.* **26,** 342 (1954).
17. J.-M. Le Meins, A. Hémon-Ribaud, J.-M. Grenèche, and G. Courbion, *in* "5th European Conference on Solid State Chemistry," Montpellier, 1995.
18. J.-M. Le Meins, G. Courbion, and J.-M. Grenèche, *Hyp. Inter.*, in press (1999).
19. C. Ninclaus, "TILT-M.E.T., A Help for Reciprocal Lattice Reconstitution." Laboratoire des Fluorures, Université du Maine, 1996.
20. O. V. Yakubovich and O. K. Mel'nikov, *Kristallografiya* **41**(4), 663 (1996).
21. J.-M. Le Meins, and G. Courbion, to be published.
22. T. Roisnel, J. Rodriguez-Carvajal, "WINPLOTR." Laboratoire Léon Brillouin (CEA-CNRS) Centre d'Etudes de Saclay-Gif sur Yvette-France, unpublished, 1998.
23. K. Brandenburg, "DIAMOND-2.0, Visual Crystal Structure Information System." Crystal Impact Distribution, Bonn, Germany, 1998.
24. G. L. Starova, S. K. Filatov, and G. L. Matusevich, *Mineral. Mag.* **59,** 159 (1995).
25. A. Ziadi, G. Thiele, and B. Elouadi, *J. Solid State Chem.* **109,** 112 (1994).
26. K. Holz, F. Obst, and R. Mattes, *J. Solid State Chem.* **90,** 353 (1991).
27. H. R. Tietze, *Aust. J. Chem.* **34,** 2035 (1981).
28. D. Riou and G. Férey, *Eur. J. State Inorg. Chem.* **31,** 25 (1994).
29. J.-M. Le Meins, J.-M. Grenèche, G. Courbion, *J. Mag. Mag. Mat.*, in press (1999).
30. P. G. Nagornyi, A. A. Kapshuk, Z. I. Kornienko, V. V. Mitkevich, and S. M. Tretiak, *Zh. Neorg. Khim.* **35,** 389 (1990).
31. J.-M. Le Meins, O. Bohnke, and G. Courbion, *Solid State Ionics* **11,** 67 (1998).